

ARTICLE OPEN



Metagenomic insights into nutrient and hypoxic microbial communities at the macrofouling/steel interface leading to severe MIC

Zhengquan Wang^{1,2,3}, Xiutong Wang^{1,2,3}✉, Yanliang Huang^{1,2,3} and Baorong Hou¹

Adherent macrofouling in marine environments caused complex corrosion of steel surfaces, resulting in localized corrosion at the oyster/steel interface and uniform corrosion at the ascidian/steel interface. Sulfate-reducing bacteria (SRB) have been implicated in the microbiologically influenced corrosion (MIC) process at macrofouling-covered interfaces. To better understand the role of marine biofilms as key mediators in the MIC process, metagenomic techniques were used to study microbial communities and their response to macrofouling's coverage. Compared to ascidians, the formed local anaerobic zone at oyster/steel interface stimulated the growth of SRBs, leading to higher FeS content and severe localized corrosion. SRB *Desulfovibrio* and *Desulfobulbus*, along with the SRB-related functional gene *dsr*, were found to increase, while oxygen-related function genes *coxC*, *ccoN*, *ccoO*, *ccoP*, and *ccoQ* decreased. In contrast, steel surfaces without macrofouling coverage had the richest microbial communities, yet experienced less severe MIC, suggesting no direct connection between microbial abundance/diversity and steel corrosion promotion.

npj Materials Degradation (2023)7:41 | <https://doi.org/10.1038/s41529-023-00365-2>

INTRODUCTION

Marine fouling organisms refer to the general term for animals, plants, and microorganisms attached to the surface of marine facilities. Based on body size, they are classified into microfouling organisms (micron-scale) and macrofouling organisms (centimeter-scale)^{1–3}. Fouling organisms can adversely affect marine infrastructures such as ships, bridges, oil platforms, and pipelines^{3–6}. Currently, there are two main research directions regarding the relationship between biofouling and metal marine corrosion.

First, study the effect of microorganisms on metal marine corrosion. Microorganisms are believed to contribute significantly to the process of metal rusting. Biofilm-forming microorganisms can quickly colonize metal surfaces to form a highly complex, dynamic three-dimensional (3D) structure that can accelerate or inhibit MIC^{7,8}. Currently, research on marine corrosive microorganisms mainly focuses on culturable bacteria in the laboratory to study the effects of mixed or single colonies on metal corrosion under simulated field environments or controlled experimental conditions^{9–11}. A considerable number of articles have investigated the effects of sulfate-reducing bacteria (SRB)^{12–15}, nitrate-reducing bacteria (NRB)^{16–18}, acid-producing bacteria (APB)¹⁹, and iron bacteria (IB)^{20,21} on metal corrosion in the marine environment. Under anoxic conditions, SRB are commonly considered the main culprits of MIC¹⁴, which can use sulfate as a terminal electron acceptor to degrade organic compounds, leading to the production of corrosive sulfides^{12–15}. Gu et al.^{22,23} classified anaerobic MIC attacks into two different types: extracellular electron transfer MIC (EET-MIC) caused by the respiration of microbes, and metabolite MIC (M-MIC) caused by the secretion of corrosive metabolites. Recently, research on the mechanism of MIC has become increasingly in-depth. Zhou et al.²⁴ found *Shewanella oneidensis* MR-1, an attractive model microbe, can directly consume electrons from iron-containing metals under aerobic conditions. The findings demonstrate that corrosion can occur

through a significant pathway of direct electron transfer between metal and microbe. Anaerobic corrosion via flavins or H₂ as electron shuttles as well as direct electron uptake from Fe⁰ have all been proposed as potential mechanisms for corrosion by *S. oneidensis* and related species^{25–28}. Tang et al.²⁸ found that stainless steel corrosion via direct iron-to-microbe electron transfer by *Geobacter sulfurreducens* and *Geobacter metallireducens*, which are electro-trophs that are known to directly accept electrons from other microbes or electrodes. Another representative marine electro-active bacterium, *Pseudomonas aeruginosa*, a pervasive bacterium competent for developing biofilms in marine habitats has been confirmed to cause severe MIC on carbon steel through extracellular electron transfer (EET)^{29–31}. Zhou et al.³¹ found that the biocorrosion of stainless steel in marine water was accelerated via extracellular electron transfer encoding gene *phzH* of *Pseudomonas aeruginosa*. However, since there are 10⁵–10⁶ species of microorganisms in the environment, studying a single microorganism is limiting. Therefore, analyzing microbial communities in the corrosive marine environment also makes a significant contribution to research on marine MIC^{32,33}. High-throughput sequencing technology provides a good idea. High-throughput sequencing, which differs from traditional Sanger (dideoxy) sequencing, is a technique that can parallel sequence a large number of nucleic acid molecules at once^{34–38}. Typically, a single sequencing reaction can produce sequencing data of no less than 100 Mb. Procopio et al.³⁸ proposed that when combined with sequencing data from environmental samples, methodologies such as metagenomics, metatranscriptome, and metabolomics will open up another horizons in understanding of the role of corrosive microbial biofilms. The emergence of high-throughput DNA sequencing techniques has facilitated the identification of microbial species that are involved in corrosion processes of alloys, both directly and indirectly³⁸. Huttunen-Saarivirta et al.³⁵ revealed dissimilarities between the stainless steel grades in

¹Key Laboratory of Marine Environmental Corrosion and Bio-fouling, Institute of Oceanology, Chinese Academy of Science, Qingdao 266071, China. ²University of Chinese Academy of Sciences, Beijing 100049, China. ³Center for Ocean Mega-Science, Chinese Academy of Sciences, Qingdao 266071, China. ✉email: wangxiutong@qdio.ac.cn

corrosion behavior and biofouling tendency in brackish seawater using high-throughput sequencing (HTP sequencing). Zhang et al.³² utilized high-throughput sequencing to investigate the microbial community in the rust layer on the metal surface after 30 months of immersion in seawater. They proposed that each metal alloy, including carbon steel, copper alloy, and aluminum alloy, would lead to the development of a distinct microbial community. In addition, different corrosion-related microbial communities formed in the inner, middle, and outer rust layers of carbon steel.

Second, study the effect of marine macrofouling organisms on metal corrosion. Macrofouling can be categorized as soft-fouling (non-calcareous algae, sponges, and ascidians, et al.) and hard-fouling (barnacles, oysters, et al.), based on the presence or absence of calcareous shells^{3,39}. It has been observed that the attachment of macrofouling can significantly damage the integrity and performance of offshore structures^{6,40,41}. For instance, the macrofouling of calcareous shells, such as oysters and barnacles, can lead to severe localized corrosion of marine facilities⁴⁰. The most common explanation for this phenomenon is that the adhesion of macrofouling creates a “biological confinement layer” on the steel surface. The interior of the layer becomes an oxygen-deficient environment, while there is sufficient oxygen outside the layer. The formation of oxygen concentration cells accelerates crevice corrosion at the interface between the macrofouling and steel³.

However, the interface between macrofouling and steel forms an independent ecosystem. The main components of macrofouling secretions are proteins and polysaccharides, which create a eutrophic environment that promotes microbial growth^{42–45}. Perme et al.⁴⁶ found that severe localized corrosion of underwater steel bridge piles in Florida was related to corrosion influenced by macrofouling and microorganisms. They also found that cracks formed by macrofouling pollutants have a significant impact on the growth of SRB and the development of MIC. The MIC process dominated by SRB develops rapidly in enclosed environments occupied by macrofouling organisms⁵. Therefore, to study the corrosion affected by macrofouling coverage, it is necessary to establish the steel corrosion mechanism under the synergistic effect of microbial community and macrofouling, by examining the interface corrosion behavior and the abundance and diversity of microorganisms.

In this study, we investigated the corrosion behavior of high-strength low-alloy steel surfaces covered by oysters (representative of hard-fouling organisms) and ascidians (representative of soft-fouling organisms) using field immersion experiments and laboratory characterization. We used high-throughput sequencing technology to study the microbial community characteristics of the rust layer at the macrofouling/steel interface, based on the corrosion types and rust layer composition. In addition, we examined the microbial communities in oyster secretions and tissues due to their role in localized corrosion. Our results showed that the heterogeneous aerobic/anaerobic microenvironment formed at the interface and the nutrient source provided by macrofouling secretions lead to the growth of anaerobic bacteria and accelerate steel corrosion. This study provides insights into the synergistic effect of macrofouling and microorganisms on steel corrosion and contributes to the study of the close relationship between microbial growth and macrofouling.

RESULTS AND DISCUSSION

Structure of the macrofouling/steel interface

Soft-fouling and hard-fouling organisms all could pose potential threats to marine facilities. Oysters, as representatives of hard-fouling organisms, are composed of a soft body protected by two complex shell sections. The oyster shell is primarily made of 97%

calcium carbonate, which provides it with significant flexural strength and low conductivity. Ascidians, on the other hand, are representatives of soft-fouling organisms. They are highly adaptable to the environment and have strong spatial competitiveness, which allows them to quickly occupy steel surfaces and alter the diversity and structural characteristics of the original benthic community.

To investigate the corrosion behavior of steel covered by soft-fouling and hard-fouling, the steel specimens were immersed in seawater for 9 months. Then, the covered macrofouling were removed after the fouled steel specimens were collected. Different corrosion types were observed between the oyster and ascidian-covered interfaces (Fig. 1). Severe localized corrosion was observed in areas where the oysters could not fully cover due to the irregular shape of their shells, while uniform corrosion was observed on the fouled steel surface covered by ascidians.

Evidence was obtained by the SEM images and the corresponding laser confocal spectroscopy (Fig. 1). Upon removing the macrofouling, it was observed from the SEM images that for steel specimen covered by oyster (OY), a large area of peeling occurred on the outer rust layer and local damage with irregular corrosion pits were generated on this area. For steel specimen which covered by ascidians (AS), the rust layer was also dense, but a flocculent structure appeared on the upper layer of the rust. For steel specimen which not covered by macrofouling (SW), the outer rust layer was loose and easily fell off, the typical morphology of steel immersed in seawater after long-term immersion⁴⁷. It was not difficult to find that the secretion of the macrofouling penetrated into the rust layer and changed the structure of the rust layer, the coverage of the macrofouling changed the state of the outer rust layer.

Consistently, the CLSM results showed that after removing the rust layer, the OY specimen had a significantly destroyed steel surface, with significant local damage and corrosion gaps, while the AS specimen had a relatively uniform steel surface without obvious local damage. Maximum differences in corrosion depth values were extracted, and the maximum corrosion depth value for the OY specimen was 721.0 μm , far greater than the values of AS (453.048 μm) and SW (521.1 μm) specimens. The average roughness values were also analyzed, which the S_a average values of the bare steel surface sorted from largest to smallest were: OY > AS > SW. It was believed that macrofouling coverage affected the steel surface's roughness and promoted the initiation of corrosion pits. However, the gap formed by the covering environment of the oyster's calcareous shell further developed these corrosion pits, leading to severe localized damage and corrosion. In contrast, the corrosion pits promoted by ascidians coverage appeared to be connected in sheets, showing uniform corrosion.

Rust layer at the macrofouling/steel interface

The corrosion products play an important role in explaining the corrosion evolution. XPS was used to detect the elemental constituent of the rust layer formed at the macrofouling/steel interface (Fig. 2). The XPS survey scan of the corrosion products revealed that the main elements were Fe, C, O, and S. The Fe 2p high-resolution spectra (Fig. 2a) of the three specimens were decomposed to peaks at 720.1⁴⁸, 711.8⁴⁹, 725.3^{49,50}, 710.7⁵¹, and 723.5⁵² eV, related to Fe⁰, FeOOH 2p3/2, FeOOH 2p1/2, Fe₃O₄ 2p3/2, and Fe₃O₄ 2p3/2, respectively. While a peak at 713.6 eV (FeS 2p3/2)⁵⁰ were found from OY-RU and AS-RU specimens, indicating that FeS was produced at macrofouling/steel interface. This conclusion could also be confirmed by S 2p high-resolution spectra (Fig. 2d). The S 2p spectra recorded from the three specimens were composed of a common peak at 169.6 eV⁵³ corresponding to SO₄²⁻ of GR(SO₄²⁻). While corrosion products of OY-RU and AS-RU specimens were decomposed to peaks at 161.0

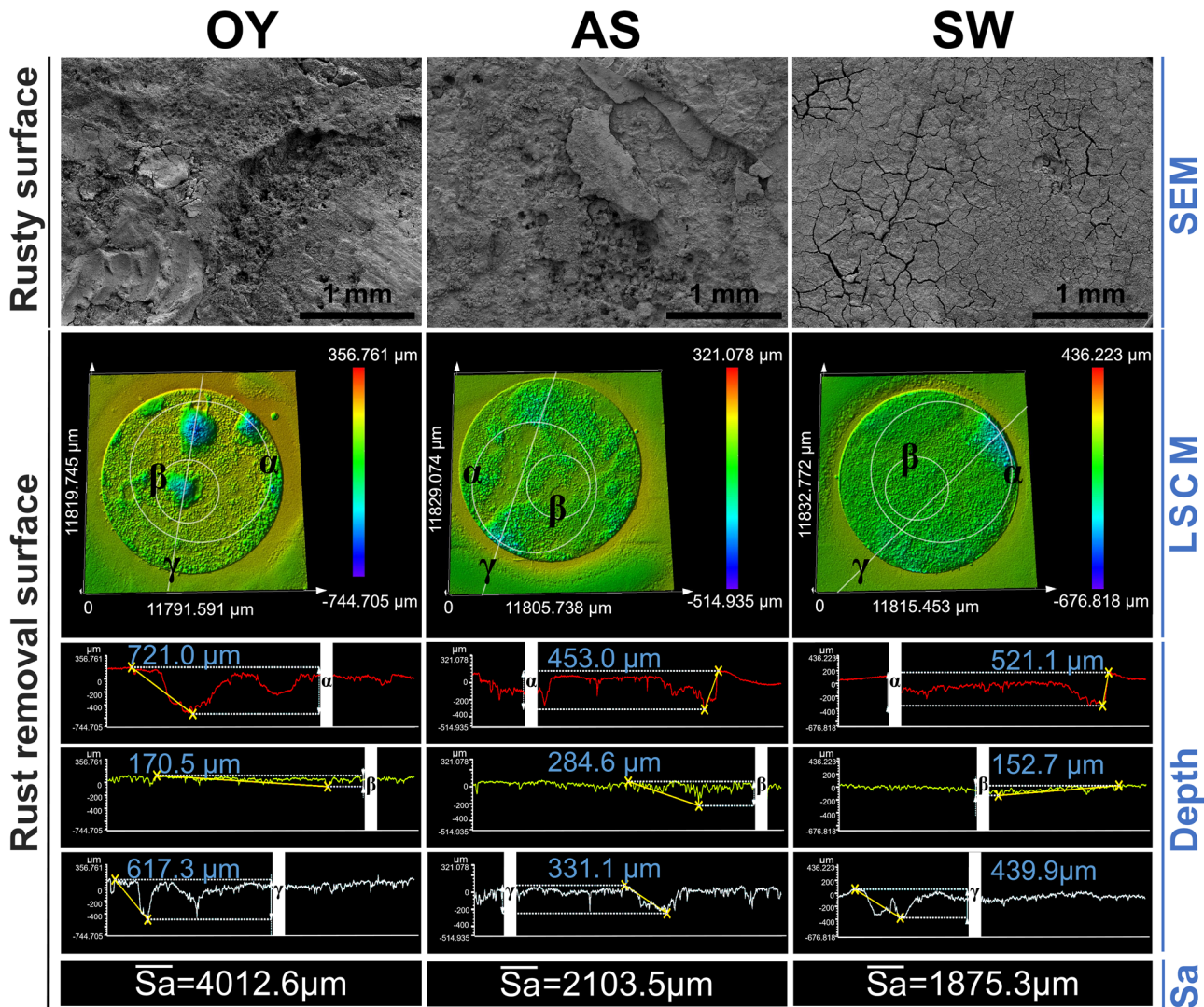


Fig. 1 Interface corrosion behavior. Macroscopic morphology analysis of the steel surface for specimens OY, AS, and SW after nine months of immersion. The SEM images corresponded to the interfacial rust morphology after removing the macrofouling, and the laser confocal spectroscopy corresponded to the whole bare steel surface morphology after removing the macrofouling and rust. OY, the steel surface covered by oysters; AS, the steel surface covered by ascidians; SW, the steel surface which not covered by macrofouling.

($S^{2-} 2p_{3/2}$) and 163.0 eV ($S^{2-} 2p_{1/2}$)⁵⁴, related to FeS. The O 1s high-resolution spectra (Fig. 2c) were decomposed to peaks at 530.0 and 531.6 eV, related to OH^- and O^{2-} , respectively⁵⁵. The C 1s high-resolution spectra (Fig. 2e) revealed three peaks: carboxylate groups ($O=C-O$) at 289.1 eV, C-C bond at 284.6 eV, and C-O bond at 286.1 eV. The C-C may result from aliphatic carbon, and C-C result from carbon single bonded to oxygen from polysaccharides or peptides/proteins^{56,57}. The carboxylate groups ($O=C-O$) may from EPS, was evidence of the accumulation of organic acids, the common bacterial metabolites entrapped within the biofilm⁵⁸. The generated EPS and FeS indicated that sulfate-reducing bacteria may be involved in the MIC process at the macrofouling/steel interface.

To further explore FeS was produced at macrofouling/steel interface, the rust layer was characterized using a Fourier transform infrared (FT-IR) spectrometer, and the resulting spectrum was examined for characteristic vibrational modes corresponding to different corrosion products (Fig. 3a). The results confirmed the presence of magnetite Fe_3O_4 , $GR(SO_4^{2-})$, lepidocrocite $\gamma-FeOOH$, akageneite $\beta-FeOOH$, goethite $\alpha-FeOOH$, and mackinawite FeS. The peak at 1020 cm^{-1} was identified as the

Fe-O vibrational mode of $\gamma-FeOOH$ ^{3,59-61}, the peaks at 795 and 885 cm^{-1} were found to be from $\alpha-FeOOH$ ^{3,59-61}, while the peaks at 420, 665, and 840 cm^{-1} were assigned to $\beta-FeOOH$ ^{3,47,61-63}. The typical Fe-O bond peaks of Fe_3O_4 were observed at 463 and 570 cm^{-1} ^{3,61,64}. In addition, peaks at 1021 and 1117 cm^{-1} were assigned to FeS ^{3,61,65,66}, while the peaks at 660 cm^{-1} were attributed to $GR(SO_4^{2-})$ ^{3,61,67,68}. The spectral bands in the range of $1400-1450\text{ cm}^{-1}$ corresponded to the symmetric stretching of C=O and deformation of O-H in COOH from proteins and polysaccharides, which have been previously reported as the primary constituents of biofilms involved in MIC^{65,69}. The presence of FeS and biofilms further supports the growth of SRB at macrofouling/steel interface.

XRD spectrum analysis was also performed on the rust layer (Fig. 3b). The results also showed that Fe_3O_4 (ICCD file 76-0958), $GR(SO_4^{2-})$ (ICCD file 13-0092), $\gamma-FeOOH$ (ICCD file 74-1877), $\alpha-FeOOH$ (ICCD file 08-0098), and $\beta-FeOOH$ (ICCD file 08-0098) were the major corrosion products in the seawater immersion environment^{70,71}. However, at the macrofouling-covered interface, the growth of SRB led to the formation of FeS (ICCD file 37-0477).

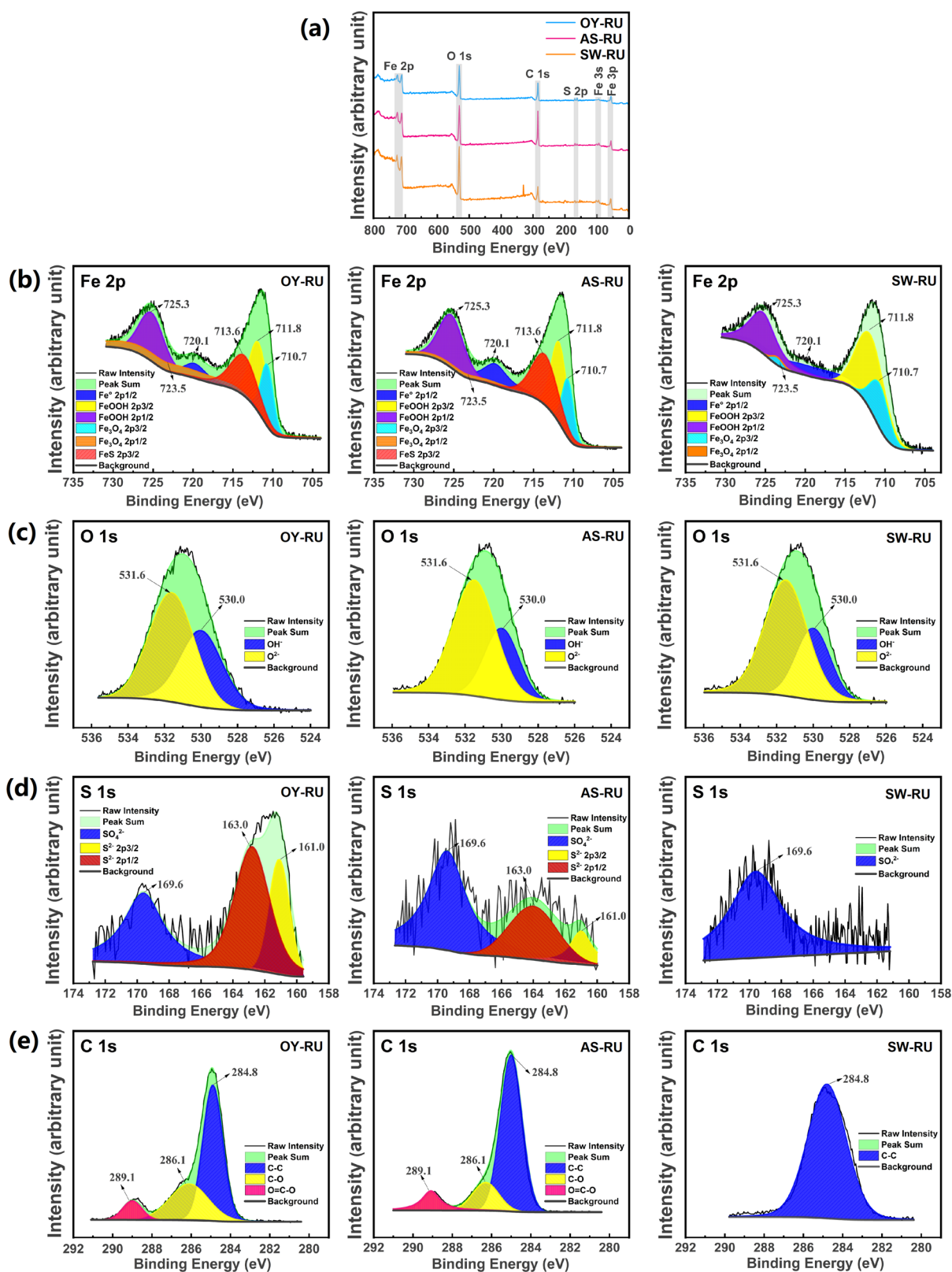


Fig. 2 XPS. XPS spectra of the rust layer formed at macrofouling/steel interface after nine months of immersion. **a** Survey scan, **b** Fe 2p high-resolution spectra, **c** O 1s high-resolution spectra, **d** S 2p high-resolution spectra, and **e** C 1s high-resolution spectra of the specimens OY-RU, AS-RU, and SW-RU. OY-RU, the rust layer or biofilm at the oyster/steel interface; AS-RU, the rust layer or biofilm at the ascidian/steel interface; SW-RU, the rust layer or biofilm at the steel interface which not covered by macrofouling.

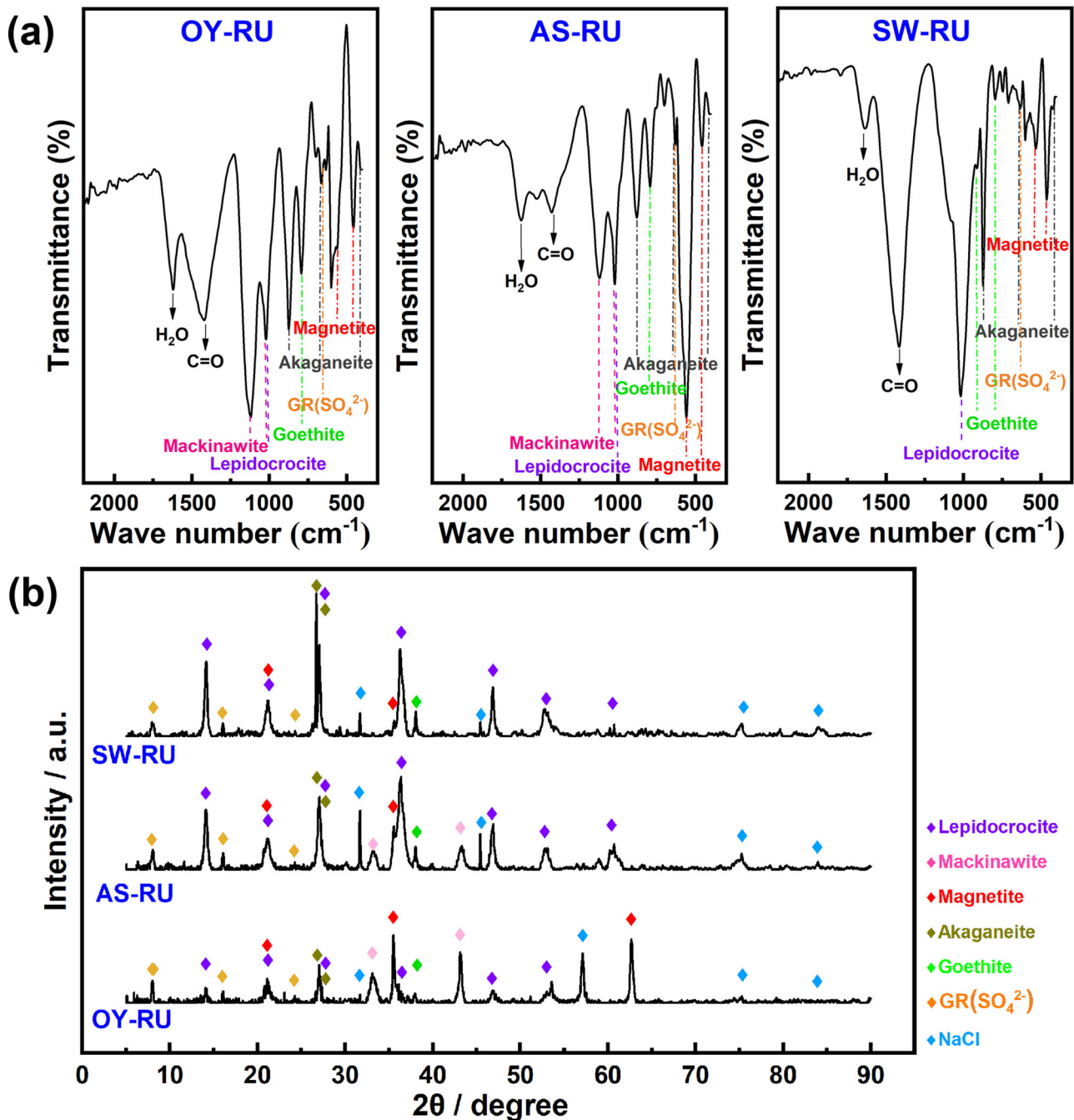


Fig. 3 FT-IR and XRD. **a** FT-IR spectra and **b** XRD spectrum of the rust layer formed at macrofouling/steel interface after nine months of immersion. OY-RU, the rust layer or biofilm at the oyster/steel interface; AS-RU, the rust layer or biofilm at the ascidian/steel interface; SW-RU, the rust layer or biofilm at the steel interface which not covered by macrofouling.

Microbial communities at the macrofouling/steel interface

Sequence analysis. Amplicon sequencing was conducted to understand the differences and dynamics of the microbial communities over time in the rust and biofilms on the steel surfaces. Using the Illumina NovaSeq sequencing platform, we obtained a total of 911,800 effective tags and 19,201 operational taxonomic units (OUTs, 97% similarity) from specimens AS-RU, OY-RU, OYS, OYT, and SW-RU (Supplementary Table 1), detecting a total of 934 genera. After analyzing the 19,201 OUTs and taking the average of parallel specimens, the flower figure and Venn diagram were obtained (Fig. 4), which showed that there were 159 OUTs shared by the five specimens. The OUTs of SW-RU were the

highest, with value of 4816. Followed by OY-RU and AS-RU, with values of 1410 and 814, respectively. It meant the rusty environment was favorable for microbial growth, corresponding to the higher abundance of microbial communities. In contrast, the abundance of microbial communities of oyster secretions was the lowest.

Alpha diversity. The α diversity of the specimens AS-RU, OY-RU, OYS, OYT, and SW-RU were analyzed to show the microbial community diversity.

The abundance and diversity index of microbial communities in biofilms and each environment were obtained (Fig. 5a and

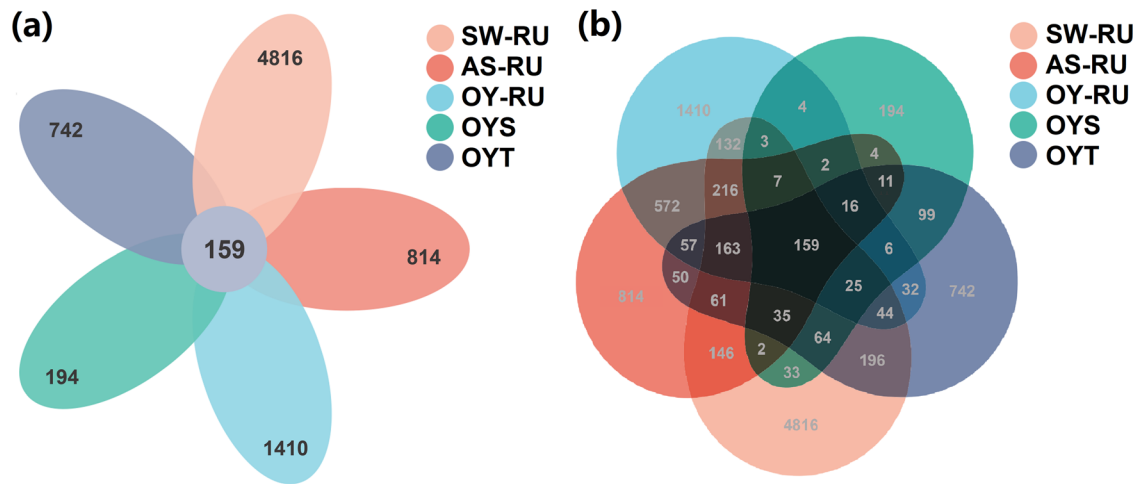


Fig. 4 Sequence analysis. **a** Flower figure and **b** Venn diagram. OY-RU, the rust layer or biofilm at the oyster/steel interface; AS-RU, the rust layer or biofilm at the ascidian/steel interface; SW-RU, the rust layer or biofilm at the steel interface which not covered by macrofouling; OYS, the biofilm in oyster's secretion; OYT, the biofilm in oyster's tissue.

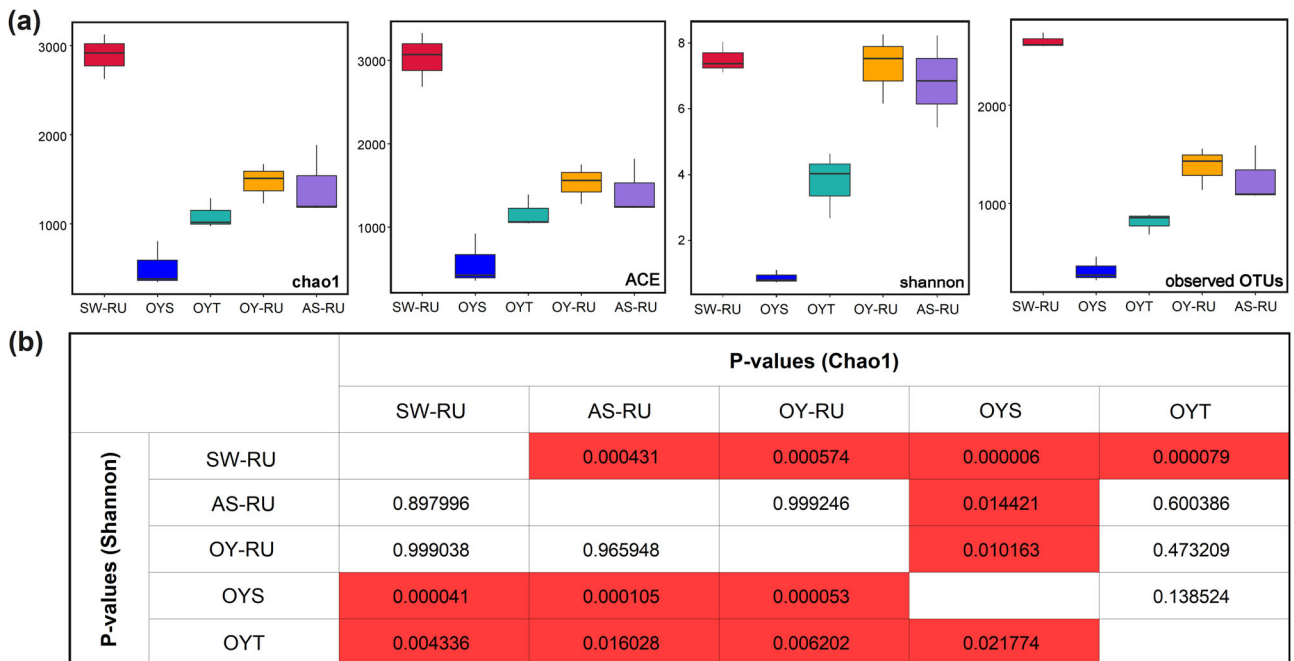


Fig. 5 α -diversity estimators. Alpha diversities estimators of microbial communities in each environment. **a** The Chao1 indices, ACE indices, Shannon indices, and observed OTUs box plots of α -diversity estimators for groups AS-RU, OY-RU, OYS, OYT, and SW-RU. The line in the middle of the box, top and bottom of the box, and whiskers represent the median, 25 and 75 percentiles, and min-to-max values, respectively. Error bars represent standard deviations of triplicate samples. **b** *p*-values for Shannon and Chao1 indices obtained using analysis of variance followed by Tukey-Kramer multiple comparison tests. The red backgrounds represent pairs with *p*-values < 0.05.

Supplementary Table 1). The values of Chao1, Ace, Shannon indexes, indices, and OTUs sorted from largest to smallest were: SW-RU > OY-RU > AS-RU > OYT > OYS. These indexes reflected information on community abundance and diversity, indicating that the microbial communities on the steel surface without macrofouling coverage had the highest abundance and diversity among the three rust layer specimens (SW-RU, OY-RU, and AS-RU). Macrofouling coverage indirectly led to a decrease in the microbial communities' abundance and diversity in the rust layer. By comparing the interfacial corrosion states of the three specimens (Fig. 1), it was believed that only a few corrosive microorganisms played key roles in the MIC process. Notably, the

OYS specimen had the lowest microbial community abundance and diversity of the three specimens associated with oysters (OY-RU, OYS, and OYT). Figure 5b showed the *p*-values for Shannon and Chao1 indices obtained using analysis of variance followed by Tukey-Kramer multiple comparison tests. These differences were statistically significant (*p* values < 0.05), indicating that the microbial communities in the rust specimens (SW-RU, AS-RU, and OY-RU) were more complex. As the rust layer was covered by macrofouling, the microbial community in the rust layer changed differentially with the gradient of oxygen concentration, and such differences in microbial diversity reflected the ecosystem at the covered interface.

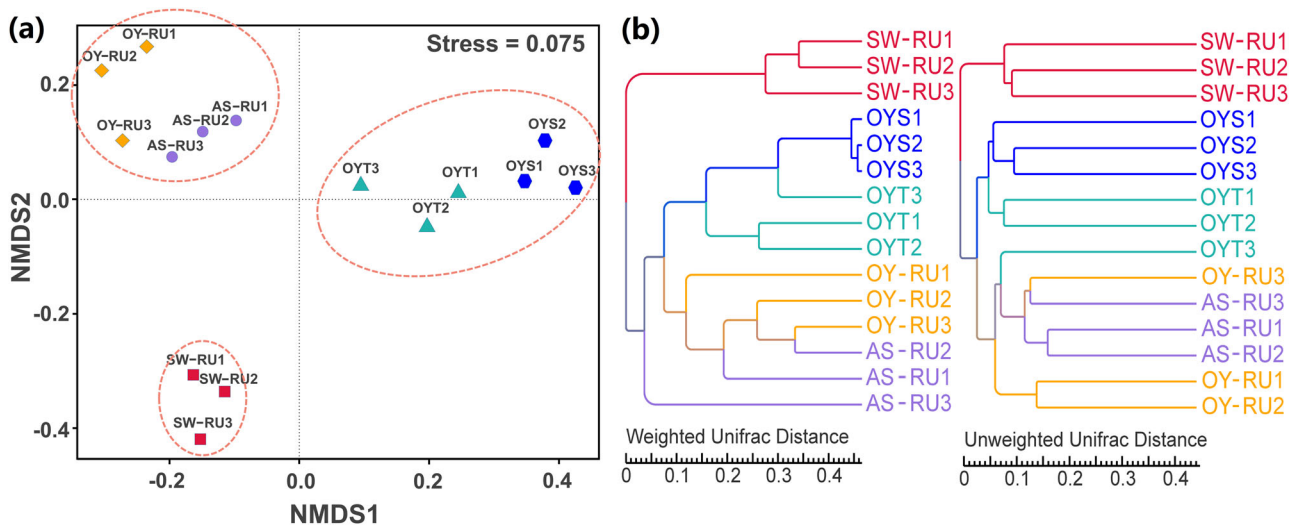


Fig. 6 β diversity. **a** Non-metric multidimensional scaling (NMDS) diagram of Bray-Curtis distances and **b** UPGMA cluster tree based on Unifrac distance and Unweighted Unifrac distance between specimens AS-RU, OY-RU, OYS, OYT, and SW-RU based on OTUs for bacteria. 1, 2, and 3 represent the three parallel specimens sampled at different sites along the interface of AS-RU, OY-RU, and SW-RU.

In addition, the rarefaction curve and rank abundance curve of 16S rRNA genes could also be used to describe the diversity of specimens (Supplementary Fig. 1). For the rarefaction curve, a flattening curve means that the amount of sequencing data is gradually reasonable, that is only a small number of new species will be generated even with more data. Rank abundance intuitively reflects the richness and evenness of species in the specimen. In the horizontal direction, the higher the species richness, the larger the span of the curve on the x-axis; in the vertical direction, the smoother the curve, the more uniform the distribution of species. As can be seen from the rarefaction curve (Supplementary Fig. 1a), the OUT Number of the rarefaction curve sorted from largest to smallest were: SW-RU > OY-RU > AS-RU > OYT > OYS, showing the same trend as Fig. 5 and Supplementary Table 1. But the curve for SW-RU specimen was not stable with more sequence number, which suggested that the diversity of bacteria of SW-RU specimen was much greater than expected. Even though the SW-RU specimens had the highest microbial abundance and diversity, their species uniformity was lower than that of the AS-RU and OY-RU specimens, as shown in rank abundance curve (Supplementary Fig. 1b). The most uneven species distribution of the OY-RU specimens also reflected that the special environment covered by the calcareous shell would lead to large differences in microbial communities.

Beta diversity. The β diversity of the specimens AS-RU, OY-RU, OYS, OYT, and SW-RU were analyzed to compare and analyze the microbial community composition between different specimens.

The non-metric multidimensional scaling (NMDS) analysis result based on the OTUs level was used to reflect the degree of difference between specimens AS-RU, OY-RU, OYS, OYT, and SW-RU through the distance between points (Fig. 6a), which can better reflect the nonlinear structure of ecological data⁷². From the NMDS results, it could be seen that the specimens OYT and OYS had obvious similarities, while specimen OY-RU and AS-RU had obvious similarities. The specimen SW-RU had a long distance, which further proved that the coverage of macrofouling led to the change of the microbial communities in the rust layer.

The UPGMA cluster tree which based on Unifrac distance and Unweighted Unifrac distance showed the same results (Fig. 6b). Specimen SW-RU contained other microbial communities which shared by the other four specimens, which meant that the special

environment of the macrofouling/steel covering interface led to the existence of characteristic microbial communities, and macrofouling secretions also shared a part of the microbial communities to a certain extent. Moreover, as the transitions in the macrofouling-covered specimens (OY-RU and AS-RU) were larger than those in the non-covered specimens (SW-RU), there was a correlation between the changes in the microbial community and corrosion progression.

Microbial communities at the phylum and class level. The relative abundance of 16S rRNA gene sequences of specimens OYT, OYS, OY-RU, AS-RU, and SW-RU at the phylum level (Fig. 7a), class level (Fig. 7b), and genus level (Fig. 7c) (relative abundance > 1%) were obtained to analyze the composition of microbial community. A total of 82 phyla, 171 classes, and 934 genera were detected.

The major phyla of microbial communities observed in the five specimens were *Proteobacteria* (38.6–96.7%), *Firmicutes* (1.5–96.7%), *Cyanobacteria* (–10.2%), *Bacteroidota* (–10.2%), *Campylobacterota* (–5.3%), *Desulfobacterota* (–5.3%), *Actinobacteriota* (–2.7%), *Actinobacteria* (–3.0%), *Verrucomicrobiota* (–1.6%), and their relative abundances vary from specimen to specimen (Fig. 7a), e.g., *Proteobacteria* and *Firmicutes* were jointly detected from all the specimens, *Bacteroidetes* shared by the specimens OYT, OY-RU, AS-RU and AS-RU. Except for these three phyla, the rust layer at the macrofouling/steel interface had richer community distribution, which *Campylobacterota*, *Actinobacteria*, and *Verrucomicrobiota* shared by the specimens OY-RU and AS-RU. Notably, OY-RU had phylum *Desulfobacterota* and *Actinobacteria*, the coverage environment by the calcareous shell of oysters resulted in a decrease in the relative abundance of *Proteobacteria* and *Bacteroidota* in the rust layer, they were replaced by *Desulfobacterota*. Such differences may be influenced by the oxygen concentration and secretions states. As almost all species of *Desulfobacterota* are SRBs^{73,74}, proving that the environment at oyster/steel interface was anaerobic. *Desulfobacterota* has been proved the main bacteria which accelerated localized corrosion, which well explained the FeS generated at the oyster/steel interface, and it was believed that *Desulfobacterota* is involved in the formation of corrosion pits at the interface to a certain extent. Besides *Desulfobacterota*, *Proteobacteria*, and *Bacteroidetes* had been proved to be the main dominant phyla at the corroded steel surface in the marine environment⁸. Most microorganisms related to iron and sulfur redox cycles belonged to the *Proteobacteria*⁷⁵. Some

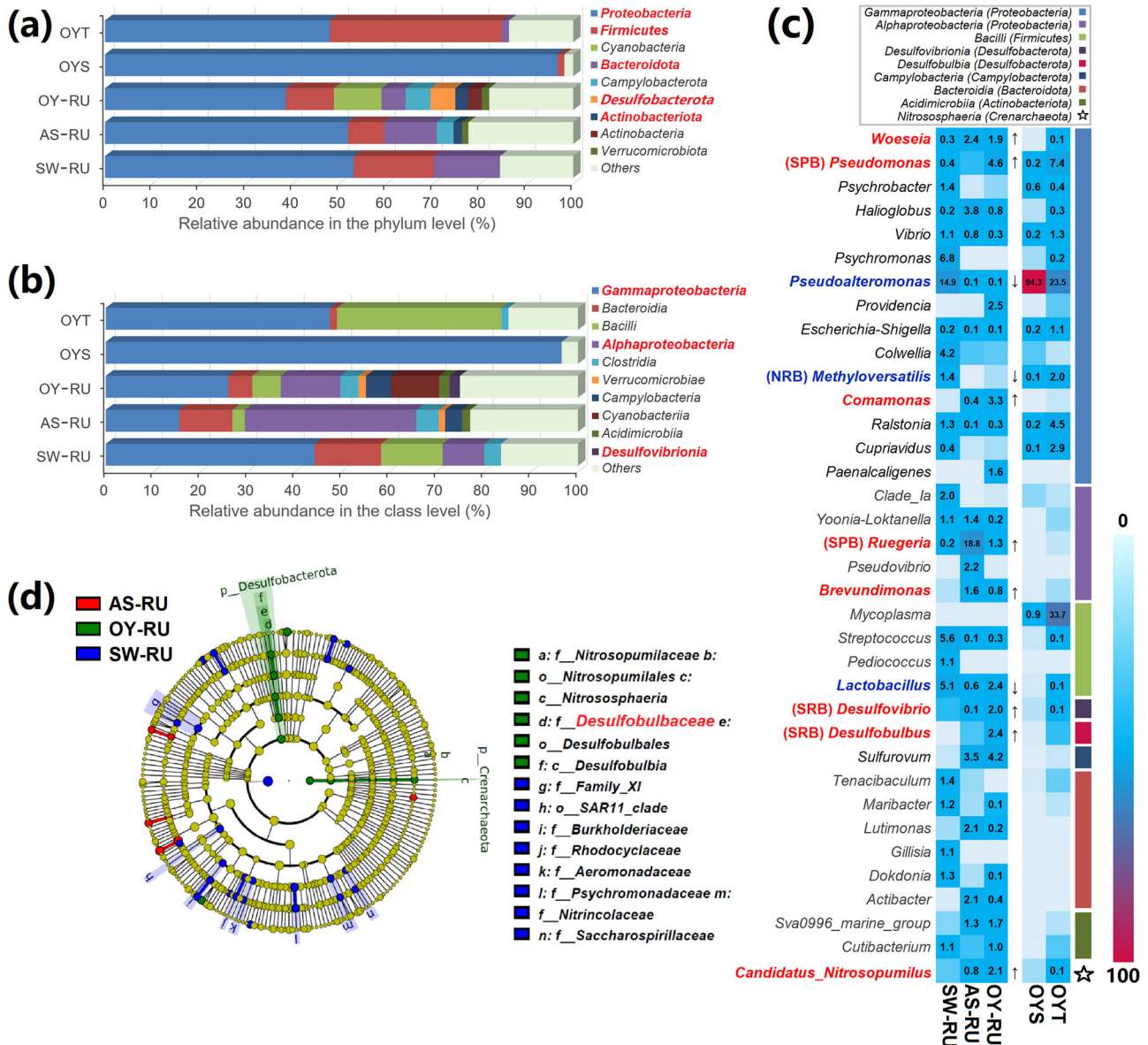


Fig. 7 Taxonomic composition. Taxonomic composition of the microbial community. **a** Phylum level, **b** class level, and **c** genus level composition analysis of top bacterial 16S rRNA gene sequences (relative abundance >1%) obtained from specimens OYT, OYS, OY-RU, AS-RU, and SW-RU. **d** The cladogram of discriminatory taxa identified in the rust-related groups (OY-RU, AS-RU, and SW-RU) by LEfSe analysis (Linear Discriminant Analysis (LDA), log score >3.5, $P = 0.05$). The relative abundance of each taxonomy was the average value of that in triplicates.

bacteria in *Proteobacteria* are very important for the formation of biofilms⁷⁶. *Bacteroidetes* was confirmed the dominant phylum in the biofilm on steel surface for short-term immersion in seawater⁷⁷. Bacteria in *Bacteroidetes* contains a large number of coding genes, which are good at using biofilms to degrade complex polymers (such as POmp and DOM) to create an anaerobic environment⁷⁸. Bacteria in *Firmicutes* and *Actinobacteria* are mostly found in pipeline environments, including various Gram-positive bacteria which can produce spores to resist dehydration and extreme environments⁷⁹. *Actinobacteria* is also one of the important microorganisms in the energy transmission pathway, which can survive in harsh environments and cause pitting corrosion^{79,80}.

Among the top 10 classes ranked according to their relative abundance (Fig. 7b), class *Gammaproteobacteria* was detected from all the specimens, classes *Bacteroidia*, *Bacilli*, and *Clostridia* shared by the specimens OYT, OY-RU, AS-RU, and SW-RU. Notably, class

Alphaproteobacteria shared by rust specimens OY-RU, AS-RU, and SW-RU. Classes *Verrucomicrobiae*, *Campylobacteria*, and *Acidimicrobiia* shared by the specimens covered by macrofouling (OY-RU and AS-RU). Apart from these, OY-RU had classes *Cyanobacteria* and *Desulfovibrionia*. Among these classes, classes *Gammaproteobacteria* and *Alphaproteobacteria* belonged to phylum *Proteobacteria*, classes *Bacilli* and *Clostridia* belonged to phylum *Firmicutes*, class *Bacteroidia* belonged to phylum *Bacteroidota*, class *Verrucomicrobiae* belonged to phylum *Verrucomicrobiota*, class *Campylobacteria* belonged to phylum *Campylobacterota*. According to the statistics, *Alphaproteobacteria* and *Gammaproteobacteria* accounted for 75% among the cultivable corrosive bacteria.

Microbial communities at the genus level. The exposure of steel in seawater and macrofouling's coverage resulted in the different formation of rust layer and biofilm between the steel surface and

the macrofouling/steel interface. The results indicated marked changes in the microbial composition, even at the genus level (Supplementary Table 2 and Fig. 7c). We focused on the top OTUs in each specimen with the relative abundance > 1%. This covered 76.5%, 94.3%, 31.1%, 39.1%, and 52.2% in specimens OYT, OYS, OY-RU, AS-RU, and SW-RU, respectively.

Usually, after microorganisms colonized the steel surface, the exopolysaccharides secreted by them would react with the organic and inorganic substances on the metal surface to form extracellular polymeric substances (EPS). The bacteria then attached to the metal surface together with EPS to form a biofilm. A major feature of biofilms is that their internal pH, dissolved oxygen (DO), ion concentration and organic content are very different from those of seawater. Generally, most marine bacteria with corrosion ability are participants in the cycle process of iron, sulfur, and other elements, and they participate in the corrosion process by changing the cathodic and anodic reaction processes on the metal surface. According to bacterial species and metabolic characteristics, the main corrosive bacteria in the ocean can be divided into sulfate-reducing bacteria (SRB), iron-oxidizing bacteria (IOB), iron-reducing bacteria (IRB), acid-producing bacteria (APB), and slime-producing bacteria (SPB), etc.

By comparing the rust biofilm specimens (SW-RU, AS-RU, and OY-RU), we found genera *Woeseia*, *Pseudomonas* (SPB), *Comamonas*, *Ruegeria* (SPB), *Brevundimonas*, *Desulfovibrio* (SRB), *Desulfohalobium* (SRB), and archaea *Candidatus_Nitrosopumilus* finally increased, but genera *Pseudoalteromonas*, *Methyloversatilis* (NRB), and *Lactobacillus* decreased with the macrofouling's coverage.

Desulfovibrio and *Desulfohalobium* are typical SRB⁸¹. SRB are heterotrophic bacteria that can directly obtain electrons from metal substrates to maintain their own life activities. SO_4^{2-} were reduced to S^{2-} due to the action of SRB, leaving a typical corrosion product FeS at macrofouling/steel interface, which was consistent with the detection of FeS in the rust layer (Fig. 2). *Desulfovibrio* belonging to class *Deltaproteobacteria* was observed as the predominant genus in the rust layer in the marine corrosion environment and has been proven to be the main cause of marine MIC^{7,13,82}. *Brevundimonas* belonging to class *Alphaproteobacteria* was one of the main microorganisms that could cause corrosion to structural steel⁸⁰. *Woeseia* was one of the facultative anaerobic microbes, which comprised facultative anaerobic, gram-negative, oxidase-negative, and catalase-positive chemoheterotrophic marine microbes⁸³. Functional microbial groups with facultative respiration mode was regarded as typical characteristics of mature biofilms in marine environments³². Biofilm-forming genera like *Pseudomonas* and *Ruegeria* dominated the surface biofilm were typical SPB. These organisms can generate an anaerobic and acidic environment. The extracellular polymer of *Lactobacillus* could change of the stability of rust layer by transferring the crystals of the carbon steel interface, which could decrease the corrosion rate of carbon steel⁸⁴. Notably, the abundance of *Pseudoalteromonas* decreased substantially with the macrofouling's coverage. This corresponded to an increase in the abundance of *Desulfovibrio*. Wu et al.⁸⁵ studied the corrosion of *Desulfovibrio* and *Pseudoalteromonas* on low carbon steel Q235 in natural seawater, and found that *Pseudoalteromonas* depleted DO in seawater, which provided the basic conditions for *Desulfovibrio*'s life activities and caused microbial corrosion. The depletion of DO changed the dominant bacteria in the rust layer from aerobic bacteria to anaerobic bacteria, so that the steel surface began to be affected by MIC. *Methyloversatilis* was observed as one of the NRB, was proved to play an important role in MIC process of the carbon steel in synthetic bentonite pore water⁸⁶. *Comamonas* was found in natural gas pipelines, which was one of the most frequently encountered bacterial and also involved in corrosion process⁸⁷. In the case of archaea, *Candidatus_nitrosopumilus* belonging to class *Nitrososphaeria* occupied a significant position at the macrofouling/steel interface. Members of this

genus chemoautotrophically grew nitrite by aerobic oxidation of ammonia and had a high specific affinity for reduced nitrogen, which ensured that they successfully compete with heterotrophic bacterioplankton and phytoplankton. Previous studies have shown that bacteria primarily contribute to surface colonization, while archaea are rarely found. However, in the present study, archaeal members were identified from the macrofouling overlay interface. Their role in macrofouling-influenced corrosion should be re-evaluated.

LefSe was further employed to identify specific taxa that were enriched in the rust-related specimens (Fig. 7d) and oyster-related specimens (Supplementary Fig. 2). It could be seen from the results that family *Desulfurivibrionaceae* including *Desulfovibrio* was enriched in specimen OY-TU among the rust-related specimens, which further proved its important role in oyster/steel interface microbial community herein.

Taken together, the macrofouling's coverage on the steel surface caused different but persistent impacts on the composition of the original microbial community compared to the rust biofilm formed by the corrosion process of steel in the seawater environment. In the otherwise nutrient-poor seawater environment, the protein and polysaccharide contained in macrofouling secretions provided the energy required for microbial growth, which stimulated the growth of microorganisms initially attached to the steel surface. Afterwards, along with the formation of an overlying anoxic environment, the abundance of anaerobic bacteria began to increase (represented by SRB), accompanied by a shift in the diversity of microbial communities. The secretion of macrofouling organisms provides carbon source for the growth of SRB. Carbon source are nutrients used as source of carbon for the formation of microbial cells and carbon-containing metabolites. It has been demonstrated that carbon sources play a crucial role in the MIC process promoted by SRB^{88–94}. The study by Liu et al.⁸⁹ indicated that SRB can survive and grow well under organic carbon source starvation. Moreover, the longer the biofilm culture time, the faster the corrosion rate of the steel. They also studied the corrosion inhibition of steel caused by imidazoline derivative in the presence of SRB with organic carbon starvation was investigated in CO_2 -saturated seawater, found that the corrosion was inhibited by SRB with a high initial count in the absence of organic carbon. However, when the initial count of SRB decreased, the corrosion rate was accelerated⁸⁸. Zhao et al.⁹² investigated the impact of different carbon sources on sulfidogenic bacterial communities during the start-up phase of acidogenic sulfate-reducing bioreactors. They observed that the 16S rRNA gene diversity of the dominant bacterial communities in each bioreactor tended to increase when using lactate, acetate/ethanol, glucose, and molasses as carbon sources.

Potential function genes at the macrofouling/steel interface

To better identify the shift in microbial community function under macrofouling's coverage conditions, we analyzed function genes using PICRUSt prediction (Fig. 8). The effects of oysters on the interface (Fig. 8a), the effects of ascidians on the interface (Fig. 8b), and the effects of oyster secretions (Fig. 8c) were considered separately. It was found that the microbial community at the macrofouling/steel interface responded differently compared to steel surfaces without macrofouling's coverage (Fig. 8a, b). For oyster covered interface (Fig. 8a), genetic information processing ribosome biogenesis and membrane transport processing phosphotransferase system (PTS) were inhibited by covered hypoxic environment, accompanied by the metabolism oxidative phosphorylation was strongly stimulated; For ascidian-covered interface (Fig. 8b), amino acid metabolism (such as valine, leucine and isoleucine degradation, tryptophan metabolism, phenylalanine metabolism and lysine degradation), lipid Metabolism fatty acid metabolism, energy metabolism (such as oxidative phosphorylation, methane

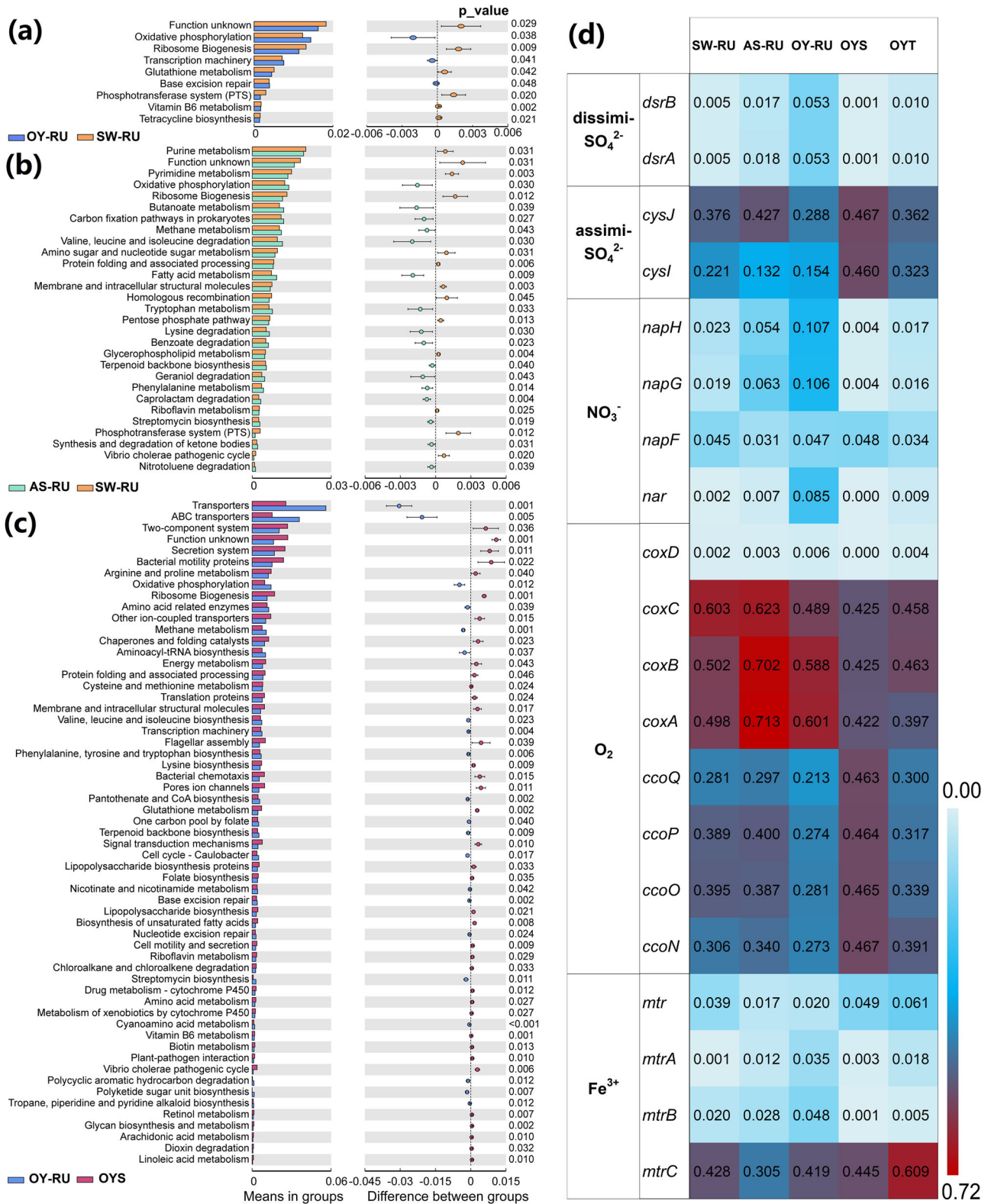


Fig. 8 Function genes. Potential functions of the microbial communities using PICRUSt prediction. The functional pathways of the microbial community by compared the groups **a** with/without oysters' coverage, **b** with/without ascidians' coverage, **c** and the microbial community from oyster secretion to the rust. The left column showed the relative abundance of each pathway and the right column showed the difference between groups. Error bars represent standard deviations of triplicate samples. **d** The abundance of important function genes related to terminal electron acceptance of the microbial community, the function of these genes can be found from Supplementary Table 3. Significant differences ($P < 0.05$) were analyzed by the T-test.

metabolism, and carbon fixation pathways in prokaryotes), xenobiotics biodegradation and metabolism caprolactam degradation, metabolism of terpenoids and polyketides geraniol degradation, and biosynthesis of other secondary metabolites (butirosin and neomycin biosynthesis and betalain biosynthesis) were strongly stimulated, accompanied by the Genetic Information Processing Ribosome Biogenesis and Membrane Transport Processing Phosphotransferase system (PTS) were also inhibited. It could be seen that the macrofouling's coverage had a certain impact on the functional pathways of the microbial community in the rust biofilm. In addition, the role of macrofouling's secretions could not be ignored (Fig. 8c). As can be seen, membrane transport (such as transporters and ABC transporters) was greatly promoted during the formation of interfacial rust biofilm.

Macrofouling's coverage changed the functional pathways of the microbial community in the rust biofilm. Thus, the key function genes related to terminal electron acceptance were further identified (Fig. 8d). It was observed that the genes related to oxygen respiration (*coxA-D* and *ccoN-Q*), denitrification (*nar* and *napF-H*), iron (*mtr* and *mtrA-C*), sulfate reduction (*dsrA,B* and *cysI,J*) were identified in all the specimens. Not surprisingly, the key gene *dsrA* and *dsrB* related to dissimilatory sulfate-reduction process were significantly stimulated in oyster covered specimens (OY-RU) ($P < 0.05$) compared to specimens AS-RU and SW-RU due to the covered anoxic environment (especially in the area covered by the oyster calcareous shell), which was consistent with the taxonomic analysis (Fig. 7). In contrast, key genes involved in assimilative sulfate reduction, such as *cysI* and *cysJ*, were reduced in specimen OY-RU ($P < 0.5$). Since the sulfate consumption of the oyster/steel interface was greater than that of the ascidian/steel interface, and greater than that of the non-fouling coverage interface. We believed that SRB reduction dissimilatory sulfate is one reason why sulfate consumption is important. Sulfate reduction by microbial assimilation could greatly facilitate the depletion of sulfate covering the anoxic interface (oyster/steel interface).

In addition to the function genes related to sulfate, this rule was also reflected in function genes such as *napH*, *napG*, *nar*, *coxC*, *ccoN*, *ccoO*, *ccoP*, and *ccoQ*. The *napH*, *napG*, and *nar* gene were significantly enriched ($P < 0.05$), and genes *coxC*, *ccoN*, *ccoO*, *ccoP*, and *ccoQ* were significantly reduced ($P < 0.05$) in rust biofilms at oyster/steel interface (OY-RU). This observation indicated that oyster covered anoxic interface stimulated the microbial denitrification, but weakened the oxygen respiration process of the microbial communities. The enhancement of the anaerobic respiration modes on steel surface was because of the formation of heterogeneous anaerobic microenvironments within the thickening and complicated rust layer, where the anaerobic areas existed. The microbial denitrification process could happen under such anaerobic conditions, which had been observed in anoxic marine environments^{7,95,96}.

Microbial communities as key mediators in the macrofouling/steel interface corrosion

In marine environment, macroorganism or microorganisms can produce localized attack as pitting, crevice corrosion at metal surface, various antifouling means are used to prevent this from happening^{97,98}. In this study, large differences in the composition and diversity of microbial communities were observed in steel surface-rust with/without macrofouling covered when we placed specimens in seawater at the same location for nine months. Meanwhile, interface morphology observation results demonstrated that the adherent oysters and ascidians had caused complex marine corrosion of fouled steel surface, manifested as local corrosion at oyster/steel interface, while the uniform corrosion at ascidian/steel interface. And the rust composition results showed that in addition to goethite, akageneite, lepidocrocite, magnetite, and $\text{GR}(\text{SO}_4^{2-})$, mackinawite was only generated at

macrofouling/steel interface. All of these implied that MIC had occurred at the macrofouling/steel interface, and the SRB were involved in the accelerated corrosion process. Therefore, we conducted a comparative study on the composition and potential functions of the microbial community in the macrofouling-covered interface-rust. The three sets of specimens SW-RU, OY-RU, and AS-RU provided data support for the quantitative analysis of the microbial community in the macrofouling-covered interface rust layer biofilm and the contribution of the microbial community to the interface corrosion process.

Our early results showed that for oyster covered interface, due to the existence of the "shadowing effect", the tightly adhered oyster calcareous-shell hindered the diffusion of oxygen and substances at the tightly-covered-area of the interface, leading to the formation of an oxygen concentration cell, thereby further accelerating the corrosion rate at where the crevice has formed³. The most critical of this process not only determined the cathodic process of metal corrosion, but also determined the composition of microorganisms in the rust-biofilm due to the change of oxygen concentration. In this research, compared to specimen not covered by macrofouling (SW-RU), different microbial communities and significant localized corrosion were observed in the rust layer biofilms on the oyster covered interface (OY-RU) (Fig. 1), strongly suggesting that such corrosion was related to MICs. With oysters covered the steel surface, SRB was easily enriched in this environments because of the high concentrations of sulfate ions^{82,99}, which was proved by the enriched SRB (Fig. 7) and key corresponding gene *dsr* (Fig. 8). The high sulfate consumption and high microbial sulfate-reduction at oyster/steel interface rust biofilms which meant the anaerobic environments for SRB was created due to the "shadowing effect" of the calcareous shell. SRB-induced MIC promoted the formation and development of corrosion pits, which induced the reduction of sulfate in seawater, and accompanied by FeS generation. We hence proposed that in corrosion processes affected by oyster, the SRB was not the main reason for the occurrence of MIC of steel in seawater until the oyster larvae began to colonize at the rusted steel surface. During oyster colonization, biofilm-forming genera (SPB) *Pseudomonas* and *Ruegeria* firstly attached to the steel surfaces and formed the biofilm. After oysters colonized the steel surface with the formation of localized anaerobic zones and heterogeneous microenvironments in the covered area, SRB- and SPB-associated bacteria proliferated and promoted the transition of rust biofilms (Fig. 7). These could be explained why anaerobic NO_3^- reduction-related genes were significantly enriched ($P < 0.05$), and genes *coxC*, *ccoN*, *ccoO*, *ccoP*, and *ccoQ* were significantly reduced (Fig. 8d), accompanied by SRB enrichment at oyster overlay interfaces (Fig. 7). These factors accelerated the crevice corrosion at oyster/steel interface.

Nobly, these phenomena did not lead to the same crevice corrosion at the ascidian/steel interface. This can be explained by the abundance of dominant microorganisms and the differences in oxygen concentration at the ascidian/steel and oyster/steel interfaces. Beneath the covered ascidian was still an aerobic environment due to the conductivity- and ion-diffusivity ability of ascidian's body. High concentration of oxygen led to the low activity of SRB, so SRB is rarely involved in the MIC process at the ascidian/steel interface. Conversely, the existing gaps at the oyster/steel interface and nutrients provided by secretions resulted in a high activity of SRBs, which caused the severe MIC at specific sites.

In summary, field experiments, laboratory characterizations, and high-throughput sequencing technology were utilized to investigate potential microbial communities at the macrofouling/steel interface, which can lead to severe microbiologically influenced corrosion (MIC). The study found that the microecological environment covered by macrofouling, as well as the nutrient source provided by macrofouling secretions, stimulated the abundance and diversity of microbial communities at the interface. Specifically, sulfate-reducing bacteria (SRB) were found to be

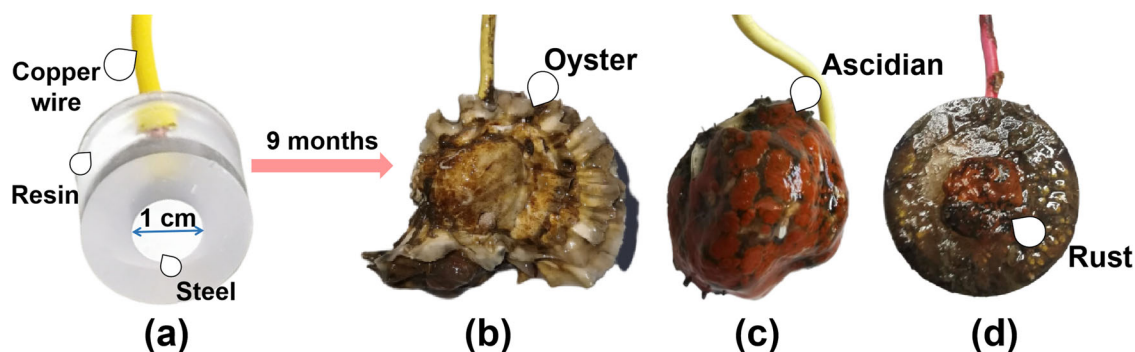


Fig. 9 Specimen collection. **a** Cylindrical specimen; **b–d** Cylindrical specimen **b** covered by an oyster, **c** covered by ascidians, and **d** not covered by macrofouling after nine months of immersion in seawater.

involved in the MIC process. MIC processes were found to differ significantly between hard-fouling and soft-fouling covered interfaces. In comparison to ascidians, the oyster/steel interface created a local anaerobic zone due to the low-ionic-diffusivity of the oyster's calcareous shell. This anaerobic environment stimulated the growth of SRBs, leading to higher FeS content and severe localized corrosion. Notably, the SRBs *Desulfovibrio* and *Desulfobulbus*, as well as the SRB-related function gene *dsr*, were increased, while the oxygen-related function gene *coxC*, *ccoN*, *ccoO*, *ccoP*, and *ccoQ* were found to decrease.

The paper did not provide data to support the hypothesis that higher microbial abundance and diversity directly promote steel corrosion. Surprisingly, the study found that steel surfaces without macrofouling coverage had the richest microbial communities, yet experienced less severe MIC. We believed that only a small fraction of the numerous microbial communities present was actually involved in the interfacial MIC process, with SRB playing a key role. The microbial community differences due to changes in the local microenvironment and the growth of anaerobic bacteria should be paid attention to during the MIC process. Doing so will help us better understand the localized corrosion mechanism at the interface and accurately quantify the specific contribution of microorganisms in complex corrosion processes.

METHODS

Material and specimen collection

High-strength low-alloy steel (AISI 4135, Shougang New Steel Co., Ltd, China) was selected as test steel in this work, which with the following element composition (in wt%): C 0.399, S 0.0144, P 0.0146, Si 0.293, Mo 0.204, Mn 0.509, Ni 0.0804, Cr 0.903, and Fe balance. Cylindrical specimens with a diameter of 1 cm and thickness of 1 cm were chosen and embedded in resins, exposing a surface area of 0.785 cm² (Fig. 9a). These specimens were then immersed in the seawater below the low tide line, where macrofouling was more likely to adhere. The field exposure site was located off a pier in Jiaozhou Bay, Qingdao, China (N 120°15'4", E 35°59'11"). After nine months of immersion in seawater from March 1, 2021 to December 1, 2021, the cylindrical specimen which covered by an oyster (Fig. 9b), covered by ascidians (Fig. 9c), and not covered by macrofouling (Fig. 9d) were retrieved. Because the attachment of macrofouling organisms is uncontrollable, the experimental design is as follows: multiple parallel specimens were hung at the same location, and the coverage of macrofouling was observed at regular intervals. After identifying some specimens with oyster and ascidian attachment, they were selected as target specimen. After a period of time, the target specimens with oyster and ascidian attachment were collected separately, and specimens without macrofouling attachment were also chosen and collected as the control group. Then, in-situ rust layers and biofilms were collected at the macrofouling/steel

interface for further sequencing and rust compositional analysis. After collecting the specimen, all the rust specimens and biofilm were transferred to sterile centrifuge tubes¹⁰⁰. Three parallel specimens were collected at different points and were assigned SW-RU (the rust layer or biofilm at the steel interface which not covered by macrofouling), AS-RU (the rust layer or biofilm at the ascidian/steel interface), OY-RU (the rust layer or biofilm at the oyster/steel interface), OY (the rust layer or biofilm in oyster secretions), and OYT (the rust layer or biofilm in oyster tissues). For rust specimens (SW-RU, OY-RU, and AS-RU), first removed the covered macrofouling from the steel substrate surface, and then collect the rust layer and biofilms with sterile forceps. For OYS and OYT specimens, first used sterile forceps to pry open the oyster shell. Then, used a sterile pipette to collect the oyster secretions (OYS) and used a sterile surgical blade to cut and collect the oyster tissues (OYT). All collected specimens were kept in an ice box, transported to the laboratory as soon as possible, and stored at −20 °C for further analysis.

Interface morphology observation and rust layer analysis

For macrofouling/steel interface morphology observation and rust layer analysis, the covered macrofouling were removed first and then the rust composition and morphology characterization of macrofouling/steel interface were carried out. The morphology of the rust-covered steel surface after removing the macrofouling was investigated by scanning electron microscopy (SEM, Regulus 8100, Hitachi, Japan). The rust-removed steel surface was observed by a 3D measuring laser microscope (LSCM, LEXT 3D OLS5000, Olympus, Japan) after removed the rust layer by using 20 vol% hydrochloric acid with 1 vol% hexamethylenetetramine. The collected rust layer was mixed with glycerol and freeze-vacuum dried to avoid oxidation and kept in vacuum containers. X-ray photoelectron spectroscopy (XPS, EscaLab 250Xi, Thermo Fisher Scientific, America), X-ray diffraction (XRD, Ultima IV, Rigaku, Japan), and Fourier transform infrared spectroscopy (FT-IR, Nicolet iS10, Thermo Fisher Scientific, USA) techniques was used for rust characterization. For XPS analysis, the XPS data were collected using a Thermo Fisher ESCALAB 250Xi spectrometer with monochromatic Al K α radiation and argon-assisted charge compensation. A step size of 0.05 eV, dwell time of 100 ms, and pass energy of 10 eV were used for the detailed spectra. Calibration was conducted to eliminate voltage-induced alterations in electron spectra. The spectra were recorded at a take-off angle of 90° and all binding energies were charge-corrected to the C 1s signal, which was set at 284.6 eV. For the characterization of the iron oxides, high-resolution scans of the C 1s, S 1s, O 1s, and Fe 2p peaks were acquired. For XRD analysis, the rust samples were characterized using a Rigaku XRD diffractometer with a Cu K α radiation ($\lambda = 1.5406 \text{ \AA}$). The diffraction data were collected over a 2θ range of 5–90° with a scanning rate of 5°/min. For FT-IR analysis, the rust sample was ground into a fine powder and pressed into a disc using

spectroscopically pure dry KBr under vacuum. Spectra was collected over a range of wavelengths ($400\text{--}4000\text{ cm}^{-1}$) at a resolution of 2 cm^{-1} . Background spectra was collected prior to each individual sample.

DNA extraction and sequencing

DNA extracted from the specimens by the SDS method was used for sequencing, then agarose gel electrophoresis was used to check the purity and concentration of DNA. Specific primers with Barcode, Phusion® High-Fidelity PCR Master Mix with GC Buffer (New England Biolabs, England), and high-efficiency high-fidelity enzymes were used for PCR amplification¹⁰¹. 16S rRNA genes were amplified using the primer sets 515F/806R. The integrity and approximate length of the DNA were examined by 2% agarose gel electrophoresis, and PCR products were purified with a PCR purification kit (QIAGEN, Hilden, NRW, Germany)^{102,103}. The PCR libraries were conducted using TruSeq® DNA PCR-Free specimen Preparation Kit (Illumina, San Diego, CA). After quantification with Qubit and Q-PCR quantification, the qualified PCR libraries were sequenced on the Illumina NovaSeq6000 platform.

Sequence data analysis

After truncating the Barcode and primer sequences according to the Barcode sequence and PCR amplification primer sequence, FLASH (V1.2.7) was used to splice the reads of each specimen to obtain raw tags¹⁰⁴. The quality control was performed on the raw tags (sequence length is 200 to 10,000 base pairs, consecutive identical base pairs $N < 6$; fuzzy bases $N < 1$, $Q < 25$), then the Fastp software was used to filter the spliced raw tags to obtain clean tags. After removing chimeric sequences, the fine effective tags were obtained¹⁰⁵. For OTU subsequent diversity index and abundance information analysis, the Uparse algorithm (Uparse v7.0.1001)¹⁰⁶ was used to cluster all effective tags of all specimens and the sequences were clustered into OTUs (operational taxonomic units) with 97% sequence similarity. Species annotation was performed on OTUs sequences, and species annotation analysis was performed using the Mothur method and the SSUrRNA database (SILVA138.1)^{107,108} to obtain taxonomic information and community composition at each taxonomic level: kingdom, phylum, class, order, family, genus, species.

The alpha diversity index (α diversity) was used to indicate the microbial community diversity within specimens. QIIME calculation and R software were used to cover the sequencing depth¹⁰⁹. Observed-otus, Chao1, Shannon, Simpson, and ACE indices were calculated using QIIME software (Version 1.9.1), and dilution curves and rank abundance curves were drawn using R software (Version 2.15.3)¹¹⁰. The beta diversity index (β diversity) was used to analyze the microbial community composition of different specimens. Based on the weighted non-frac distance, the Bray-Curtis distance based on OTU was drawn from the non-metric multidimensional scaling (NMDS)^{111,112}. UPGMA cluster analysis was performed with weighted unfrac distance matrix and unweighted unfrac distance matrix. The clustering results were integrated and displayed with the relative abundance of species at the phylum level in each specimen^{113,114}. Applied PCA analysis to extract two axes that best reflect the differences between specimens¹¹¹. The unfrac distance was calculated by QIIME software (Version 1.9.1), and the UPGMA specimen clustering tree was constructed. PCA and NMDS plots were also drawn using R software (Version 2.15.3). The potential function genes were annotated against KEGG database using PICRUSt prediction^{115,116}. The cladogram of discriminatory taxa was identified in the rust-related groups by the linear discriminant analysis (LDA) based on Kruskal–Wallis with log score >3.5 and $P = 0.05$ using LefSe software (V1.0)^{7,117}. The relative abundance of each taxonomy was the average value of that in triplicates. T-test was used to determine the difference in individual function genes between different treatments⁷.

DATA AVAILABILITY

The data that support the findings of this study are available from the corresponding author upon reasonable request. Sequencing data of the 15 specimens obtained were deposited in the NCBI Short Read Archive (SRA) database under Bioproject accession number PRJNA865886, with Biospecimen numbers SAMN 30139936–30139950.

Received: 19 January 2023; Accepted: 12 May 2023;

Published online: 24 May 2023

REFERENCES

- Guenther, J., Walker-Smith, G., Waren, A. & De Nys, R. Fouling-resistant surfaces of tropical sea stars. *Biofouling* **23**, 413–418 (2007).
- Myan, F. W. Y., Walker, J. & Paramor, O. The interaction of marine fouling organisms with topography of varied scale and geometry: a review. *Biointerphases* **8**, 30 (2013).
- Wang, Z. Q., Huang, Y. L., Wang, X. T., Xu, Y. & Cai, F. F. Effects of oyster as macrofouling organism on corrosion mechanisms of a high-strength low-alloy steel. *Corros. Sci.* **207**, 110580 (2022).
- Li, Y. F. & Ning, C. Y. Latest research progress of marine microbiological corrosion and bio-fouling, and new approaches of marine anti-corrosion and anti-fouling. *Bioact. Mater.* **4**, 189–195 (2019).
- Perme, S., Lau, K., Boan, M. E. & Duncan, M. Influence of macro- and micro-fouling on corrosion of steel bridge piles submerged in natural waters. *J. Mater. Civ. Eng.* **33**, 04021105 (2021).
- De Brito, L. V. R., Coutinho, R., Cavalcanti, E. S. & Benchimol, M. The influence of macrofouling on the corrosion behaviour of API 5L X65 carbon steel. *Biofouling* **23**, 193–201 (2007).
- Zhang, Y. M. et al. Microbiologically influenced corrosion of steel in coastal surface seawater contaminated by crude oil. *npj Mater. Degrad.* **6**, 35 (2022).
- Zhang, Y. M. et al. Analysis of marine microbial communities colonizing various metallic materials and rust layers. *Biofouling* **35**, 429–442 (2019).
- Lanneluc, I. et al. On the bacterial communities associated with the corrosion product layer during the early stages of marine corrosion of carbon steel. *Int. Biodeterior. Biodegrad.* **99**, 55–65 (2015).
- Cheng, S. et al. Microbially influenced corrosion of stainless steel by marine bacterium *Vibrio natriegens*: (I) Corrosion behavior. *Mater. Sci. Eng. C.* **29**, 751–755 (2009).
- Khan, M. S. et al. Microbiologically influenced corrosion of titanium caused by aerobic marine bacterium *Pseudomonas aeruginosa*. *J. Mater. Sci. Technol.* **35**, 216–222 (2019).
- Venzlaff, H. et al. Accelerated cathodic reaction in microbial corrosion of iron due to direct electron uptake by sulfate-reducing bacteria. *Corros. Sci.* **66**, 88–96 (2013).
- Duan, J. Z. et al. Corrosion of carbon steel influenced by anaerobic biofilm in natural seawater. *Electrochim. Acta* **54**, 22–28 (2008).
- Enning, D. & Garrelfs, J. Corrosion of iron by sulfate-reducing bacteria: new views of an old problem. *Appl. Environ. Microbiol.* **80**, 1226–1236 (2014).
- Dinh, H. T. et al. Iron corrosion by novel anaerobic microorganisms. *Nature* **427**, 829–832 (2004).
- Dou, W. W. et al. Biocorrosion of copper by nitrate reducing *Pseudomonas aeruginosa* with varied headspace volume. *Int. Biodeterior. Biodegrad.* **171**, 105405 (2022).
- Chugh, B. et al. Extracellular electron transfer by *Pseudomonas aeruginosa* in biocorrosion: a review. *ACS Biomater. Sci. Eng.* **8**, 1049–1059 (2022).
- Pu, Y. N. et al. Microbiologically influenced corrosion of Cu by nitrate reducing marine bacterium *Pseudomonas aeruginosa*. *J. Mater. Sci. Technol.* **47**, 10–19 (2020).
- Tian, F., He, X. Y., Bai, X. Q. & Yuan, C. Q. Electrochemical corrosion behaviors and mechanism of carbon steel in the presence of acid-producing bacterium *Citrobacter farmeri* in artificial seawater. *Int. Biodeterior. Biodegrad.* **147**, 104872 (2020).
- Chen, S. Q., Deng, H., Liu, G. Z. & Zhang, D. Corrosion of Q235 carbon steel in seawater containing *Mariprofundus ferrooxydans* and *Thalassospira* sp. *Front. Microb.* **10**, 936 (2019).
- Sun, H. F., Shi, B. Y., Yang, F. & Wang, D. S. Effects of sulfate on heavy metal release from iron corrosion scales in drinking water distribution system. *Water Res.* **114**, 69–77 (2017).
- Gu, T. Y., Wang, D., Lekbach, Y. & Xu, D. K. Extracellular electron transfer in microbial biocorrosion. *Curr. Opin. Electrochem.* **29**, 100763 (2021).
- Gu, T. New understandings of biocorrosion mechanisms and their classifications. *J. Microb. Biochem. Technol.* **4**, 1 (2012).
- Zhou, E. Z. et al. Direct microbial electron uptake as a mechanism for stainless steel corrosion in aerobic environments. *Water Res.* **219**, 118553 (2022).

25. Jin, Y. T. et al. Sharing riboflavin as an electron shuttle enhances the corrosivity of a mixed consortium of *Shewanella oneidensis* and *Bacillus licheniformis* against 316L stainless steel. *Electrochim. Acta* **316**, 93–104 (2019).
26. Li, Z. Y. et al. Adaptive bidirectional extracellular electron transfer during accelerated microbiologically influenced corrosion of stainless steel. *Commun. Mater.* **2**, 67 (2021).
27. Kalnaowakul, P., Xu, D. K. & Rodchanarowan, A. Accelerated corrosion of 316L stainless steel caused by *Shewanella algae* biofilms. *ACS Appl. Bio Mater.* **3**, 2185–2192 (2020).
28. Tang, H. Y. et al. Stainless steel corrosion via direct iron-to-microbe electron transfer by *Geobacter* species. *ISME J.* **15**, 3084–3093 (2021).
29. Reguera, G. et al. Extracellular electron transfer via microbial nanowires. *Nature* **435**, 1098–1101 (2005).
30. Pham, T. H. et al. Metabolites produced by *Pseudomonas* sp enable a Gram-positive bacterium to achieve extracellular electron transfer. *Appl. Microbiol. Biotechnol.* **77**, 1119–1129 (2008).
31. Zhou, E. Z. et al. Accelerated biocorrosion of stainless steel in marine water via extracellular electron transfer encoding gene *phzH* of *Pseudomonas aeruginosa*. *Water Res.* **220**, 118634 (2022).
32. Zhang, Y. M. et al. Metagenomic resolution of functional diversity in copper surface-associated marine biofilms. *Front. Microb.* **10**, 2863 (2019).
33. Wang, Z. Q., Li, Y. T., Ren, J., Xu, W. C. & Yang, L. H. Investigating the effects of environment, corrosion degree, and distribution of corrosive microbial communities on service-life of refined oil pipelines. *Environ. Sci. Pollut. Res.* **29**, 52204–52219 (2022).
34. Zhang, G. J. et al. The bacterial community significantly promotes cast iron corrosion in reclaimed wastewater distribution systems. *Microbiome* **6**, 1–18 (2018).
35. Huttunen-Saarivirta, E. et al. Ennoblement, corrosion, and biofouling in brackish seawater: comparison between six stainless steel grades. *Bioelectrochemistry* **120**, 27–42 (2018).
36. Staniszevska, A. et al. High-throughput sequencing approach in analysis of microbial communities colonizing natural gas pipelines. *Microbiologyopen* **8**, e00806 (2019).
37. de Azambuja, A. O. et al. Microbial community composition in Brazilian stored diesel fuel of varying sulfur content, using high-throughput sequencing. *Fuel* **189**, 340–349 (2017).
38. Procopio, L. The era of 'omics' technologies in the study of microbiologically influenced corrosion. *Biotechnol. Lett.* **42**, 341–356 (2020).
39. Lezzi, M., Del Pasqua, M., Pierri, C. & Giangrande, A. Seasonal non-indigenous species succession in a marine macrofouling invertebrate community. *Biol. Invasions* **20**, 937–961 (2018).
40. Blackwood, D. J., Lim, C. S., Teo, S. L. M., Hu, X. P. & Pang, J. J. Macrofouling induced localized corrosion of stainless steel in Singapore seawater. *Corros. Sci.* **129**, 152–160 (2017).
41. Vinagre, P. A., Simas, T., Cruz, E., Pinori, E. & Svenson, J. Marine biofouling: a European database for the marine renewable energy sector. *J. Mar. Sci. Eng.* **8**, 495 (2020).
42. Jonker, J. L. et al. The chemistry of stalked barnacle adhesive (*Lepas anatifera*). *Interface Focus* **5**, 20140062 (2015).
43. Lee, H., Dellatore, S. M., Miller, W. M. & Messersmith, P. B. Mussel-inspired surface chemistry for multifunctional coatings. *Science* **318**, 426–430 (2007).
44. Lee, H., Scherer, N. F. & Messersmith, P. B. Single-molecule mechanics of mussel adhesion. *Proc. Natl Acad. Sci. USA* **103**, 12999–13003 (2006).
45. Zhang, G. F. et al. The oyster genome reveals stress adaptation and complexity of shell formation. *Nature* **490**, 49–54 (2012).
46. Permeh, S., Lau, K., Boan, M. E., Tansel, B. & Duncan, M. Cathodic polarization behavior of steel with different marine fouling morphologies on submerged bridge elements with cathodic protection. *J. Mater. Civ. Eng.* **32**, 04020184 (2020).
47. Zou, Y., Wang, J. & Zheng, Y. Y. Electrochemical techniques for determining corrosion rate of rusted steel in seawater. *Corros. Sci.* **53**, 208–216 (2011).
48. Xu, W. C. et al. Accelerated corrosion of 316L stainless steel in simulated body fluids in the presence of H₂O₂ and albumin. *Mater. Sci. Eng. C-Mater. Biol. Appl.* **92**, 11–19 (2018).
49. Guo, S. Q., Xu, L. N., Zhang, L., Chang, W. & Lu, M. X. Corrosion of alloy steels containing 2% chromium in CO₂ environments. *Corros. Sci.* **63**, 246–258 (2012).
50. Wang, Z. Q. et al. Study on inner corrosion behavior of high strength product oil pipelines. *Eng. Fail. Anal.* **115**, 104659 (2020).
51. Marcus, P. & Grimal, J. M. The anodic dissolution and passivation of NiCrFe alloys studied by ESCA. *Corros. Sci.* **33**, 805–814 (1992).
52. Tan, B. J., Klabunde, K. J. & Sherwood, P. M. A. X-ray photoelectron spectroscopy studies of solvated metal atom dispersed catalysts. Monometallic iron and bimetallic iron-cobalt particles on alumina. *Chem. Mater.* **2**, 186–191 (1990).
53. Wren, A. G., Phillips, R. W. & Tolentino, L. U. Surface reactions of chlorine molecules and atoms with water and sulfuric acid at low temperatures. *J. Colloid Interface Sci.* **70**, 544–557 (1979).
54. Boursiquot, S., Mullet, M. & Ehrhardt, J. J. XPS study of the reaction of chromium (VI) with mackinawite (FeS). *Surf. Interface Anal.* **34**, 293–297 (2002).
55. Allen, G. C., Curtis, M. T., Hooper, A. J. & Tucker, P. M. X-Ray photoelectron spectroscopy of iron–oxygen systems. *J. Chem. Soc. Dalton Trans.* **14**, 1525–1530 (1974).
56. Rouxhet, P. G. & Genet, M. J. XPS analysis of bio-organic systems. *Surf. Interface Anal.* **43**, 1453–1470 (2011).
57. Ramstedt, M., Leone, L., Persson, P. & Shchukarev, A. Cell wall composition of *Bacillus subtilis* changes as a function of pH and Zn²⁺ exposure: insights from cryo-XPS measurements. *Langmuir* **30**, 4367–4374 (2014).
58. Kumar, M. A., Anandapandian, K. T. K. & Parthiban, K. Production and characterization of exopolysaccharides (EPS) from biofilm forming marine bacterium. *Braz. Arch. Biol. Technol.* **54**, 259–265 (2011).
59. Perez, F. R., Barrero, C. A. & Garcia, K. E. Factors affecting the amount of corroded iron converted into adherent rust in steels submitted to immersion tests. *Corros. Sci.* **52**, 2582–2591 (2010).
60. Weckler, B. & Lutz, H. D. Lattice vibration spectra. Part XCV. Infrared spectroscopic studies on the iron oxide hydroxides goethite (alpha), akaganite (beta), lepidocrocite (gamma), and ferroxite (delta). *Eur. J. Solid State Inorg. Chem.* **35**, 531–544 (1998).
61. Wang, Z. et al. Macrofouling organisms: protection or damage of steel in marine environments? *Corros. Sci.* **212**, 110928 (2023).
62. Song, H., Zhang, X., Chen, T. & Jia, X. One-pot synthesis of bundle-like beta-FeOOH nanorods and their transformation to porous alpha-Fe₂O₃ microspheres. *Ceram. Int.* **40**, 15595–15602 (2014).
63. Wei, C. & Nan, Z. Effects of experimental conditions on one-dimensional single-crystal nanostructure of beta-FeOOH. *Mater. Chem. Phys.* **127**, 220–226 (2011).
64. Hu, J. Y., Cao, S. A. & Xie, J. L. EIS study on the corrosion behavior of rusted carbon steel in 3% NaCl solution. *Anti-Corros. Methods Mater.* **60**, 100–105 (2013).
65. Badica, C. E. & Chirita, P. An electrochemical study of the oxidative dissolution of iron monosulfide (FeS) in air-equilibrated solutions. *Electrochim. Acta* **178**, 786–796 (2015).
66. Chirita, P., Descostes, M. & Schlegel, M. L. Oxidation of FeS by oxygen-bearing acidic solutions. *J. Colloid Interface Sci.* **321**, 84–95 (2008).
67. Ona-Nguemo, G. et al. Competitive formation of hydroxycarbonate green rust 1 versus hydroxysulphate green rust 2 in *Shewanella putrefaciens* cultures. *Geomicrobiol. J.* **21**, 79–90 (2004).
68. Zegeye, A. et al. Formation of hydroxysulphate green rust 2 as a single Iron(III) mineral in microbial culture. *Geomicrobiol. J.* **22**, 389–399 (2005).
69. Ferri, T. Z., Roncevic, S., Vrkljan, G. L. & Konestra, A. Post-depositional alterations of terrestrial and marine finds of Roman ceramics from Crikvenica production centre (NE Adriatic, Croatia)—a contribution towards chemometric classification. *J. Cult. Herit.* **43**, 12–25 (2020).
70. Refait, P., Grolleau, A. M., Jeannin, M., Francois, E. & Sabot, R. Localized corrosion of carbon steel in marine media: Galvanic coupling and heterogeneity of the corrosion product layer. *Corros. Sci.* **111**, 583–595 (2016).
71. Refait, P., Jeannin, M., Sabot, R., Antony, H. & Pineau, S. Electrochemical formation and transformation of corrosion products on carbon steel under cathodic protection in seawater. *Corros. Sci.* **71**, 32–36 (2013).
72. Rivas, M. N. et al. A microbiota signature associated with experimental food allergy promotes allergic sensitization and anaphylaxis. *J. Allergy Clin. Immunol.* **131**, 201–212 (2013).
73. Waite, D. W. et al. Proposal to reclassify the proteobacterial classes *Deltaproteobacteria* and *Oligoflexia*, and the phylum *Thermodesulfobacteria* into four phyla reflecting major functional capabilities. *Int. J. Syst. Evol. Microbiol.* **70**, 5972–6016 (2020).
74. Wakai, S. et al. Dynamics of microbial communities on the corrosion behavior of steel in freshwater environment. *npj Mater. Degrad.* **6**, 45 (2022).
75. Cankovic, M., Petric, I., Margus, M. & Ciglenecki, I. Spatio-temporal dynamics of sulfate-reducing bacteria in extreme environment of Rogoznica Lake revealed by 16S rRNA analysis. *J. Mar. Syst.* **172**, 14–23 (2017).
76. Park, H. I., Kim, J. S., Kim, D. K., Choi, Y. J. & Pak, D. Nitrate-reducing bacterial community in a biofilm-electrode reactor. *Enzym. Microb. Technol.* **39**, 453–458 (2006).
77. Oliveira, V. M. et al. Molecular analysis of microbial diversity in corrosion samples from energy transmission towers. *Biofouling* **27**, 435–447 (2011).
78. Conlette, O. C. Microbial communities of light crude from Nigeria and potential for in situ biodegradation, souring, and corrosion. *Pet. Sci. Technol.* **34**, 71–77 (2016).
79. Burleigh, T. D., Gierke, C. G., Fredj, N. & Boston, P. J. Copper tube pitting in Santa Fe municipal water caused by microbial induced corrosion. *Materials* **7**, 4321–4334 (2014).
80. Machuca, L. L., Jeffrey, R. & Melchers, R. E. Microorganisms associated with corrosion of structural steel in diverse atmospheres. *Int. Biodeterior. Biodegrad.* **114**, 234–243 (2016).

81. Anandkumar, B., George, R. P., Maruthamuthu, S., Palaniswamy, N. & Dayal, R. K. Corrosion behavior of SRB *Desulfohalobium propionicum* isolated from an Indian petroleum refinery on mild steel. *Mater. Corros.* **63**, 355–362 (2012).
82. Li, X. H. et al. Analysis of bacterial community composition of corroded steel immersed in Sanya and Xiamen seawaters in China via method of Illumina MiSeq sequencing. *Front. Microb.* **8**, 1737 (2017).
83. Du, Z. J., Wang, Z. J., Zhao, J. X. & Chen, G. J. *Woeseia oceani* gen. nov., sp nov., a chemoheterotrophic member of the order Chromatiales, and proposal of Woeseiaceae fam. nov. *Int. J. Syst. Evol. Microbiol.* **66**, 107–112 (2016).
84. Ignatova-Ivanova, T., Ivanov, R., Iliev, I. & Ivanova, I. Study of anticorrosion effect of EPS from now strains *Lactobacillus delbrueckii*. *Biotechnol. Biotechnol. Equip.* **23**, 705–708 (2009).
85. Wu, J. J. et al. The influence of *Desulfovibrio* sp and *Pseudoalteromonas* sp on the corrosion of Q235 carbon steel in natural seawater. *Corros. Sci.* **112**, 552–562 (2016).
86. Shrestha, R. et al. Anaerobic microbial corrosion of carbon steel under conditions relevant for deep geological repository of nuclear waste. *Sci. Total Environ.* **800**, 149539 (2021).
87. Zhu, X. Y., Lubeck, J. & Kilbane, J. J. Characterization of microbial communities in gas industry pipelines. *Appl. Environ. Microbiol.* **69**, 5354–5363 (2003).
88. Liu, H. W. et al. Corrosion inhibition behavior of X80 pipeline steel by imidazole derivative in the CO₂-saturated seawater containing sulfate-reducing bacteria with organic carbon starvation. *Corros. Sci.* **203**, 110345 (2022).
89. Liu, H. W., Gu, T. Y., Zhang, G. A., Liu, H. F. & Cheng, Y. F. Corrosion of X80 pipeline steel under sulfate-reducing bacterium biofilms in simulated CO₂-saturated oilfield produced water with carbon source starvation. *Corros. Sci.* **136**, 47–59 (2018).
90. Zhao, C. R., Chen, N., Liu, T. & Feng, C. P. Effects of adding different carbon sources on the microbial behavior of sulfate-reducing bacteria in sulfate-containing wastewater. *J. Clean. Prod.* **392**, 136332 (2023).
91. Fan, Y. X. et al. Early corrosion behavior of X80 pipeline steel in a simulated soil solution containing *Desulfovibrio desulfuricans*. *Bioelectrochemistry* **141**, 107880 (2021).
92. Zhao, Y. G., Wang, A. J. & Ren, N. Q. Effect of carbon sources on sulfidogenic bacterial communities during the starting-up of acidogenic sulfate-reducing bioreactors. *Bioresour. Technol.* **101**, 2952–2959 (2010).
93. Zhang, M. L. & Wang, H. X. Organic wastes as carbon sources to promote sulfate reducing bacterial activity for biological remediation of acid mine drainage. *Miner. Eng.* **69**, 81–90 (2014).
94. Fu, Q. et al. Biologically competitive effect of *Desulfovibrio desulfuricans* and *Pseudomonas stutzeri* on corrosion of X80 pipeline steel in the Shenyang soil solution. *Bioelectrochemistry* **145**, 108051 (2022).
95. Zedelius, J. et al. Alkane degradation under anoxic conditions by a nitrate-reducing bacterium with possible involvement of the electron acceptor in substrate activation. *Environ. Microbiol. Rep.* **3**, 125–135 (2011).
96. Scott, N. M. et al. The microbial nitrogen cycling potential is impacted by polyaromatic hydrocarbon pollution of marine sediments. *Front. Microb.* **5**, 108 (2014).
97. Zhou, Z. Y. et al. Distinctive roles of graphene oxide, ZnO quantum dots, and their nanohybrids in anti-corrosion and anti-fouling performance of waterborne epoxy coatings. *Chem. Eng. J.* **439**, 135765 (2022).
98. Zhou, Z. Y. et al. Anti-corrosion and anti-fouling properties of ball-like GQDs hybridized MOFs functionalized with silane in waterborne epoxy-polydimethylsiloxane coatings: experimental and theoretical studies. *Appl. Mater. Today* **30**, 101704 (2023).
99. Vigneron, A. et al. Complementary microorganisms in highly corrosive biofilms from an offshore oil production facility. *Appl. Environ. Microbiol.* **82**, 2545–2554 (2016).
100. Lin, W., Yu, Z., Zhang, H. & Thompson, I. P. Diversity and dynamics of microbial communities at each step of treatment plant for potable water generation. *Water Res.* **52**, 218–230 (2014).
101. Moskovitz, M. et al. Characterization of the oral microbiome among children with type 1 diabetes compared with healthy children. *Front. Microb.* **12**, 756808 (2021).
102. Di Pinto, A. et al. A comparison of DNA extraction methods for food analysis. *Food Control* **18**, 76–80 (2007).
103. Guy, R. A., Payment, P., Krull, U. J. & Horgen, P. A. Real-time PCR for quantification of Giardia and Cryptosporidium in environmental water samples and sewage. *Appl. Environ. Microbiol.* **69**, 5178–5185 (2003).
104. Magoc, T. & Salzberg, S. L. FLASH: fast length adjustment of short reads to improve genome assemblies. *Bioinformatics* **27**, 2957–2963 (2011).
105. Haas, B. J. et al. Chimeric 16S rRNA sequence formation and detection in Sanger and 454-pyrosequenced PCR amplicons. *Genome Res.* **21**, 494–504 (2011).
106. Edgar, R. C. UPARSE: highly accurate OTU sequences from microbial amplicon reads. *Nat. Methods* **10**, 996–+ (2013).
107. Wang, Q., Garrity, G. M., Tiedje, J. M. & Cole, J. R. Naive Bayesian classifier for rapid assignment of rRNA sequences into the new bacterial taxonomy. *Appl. Environ. Microbiol.* **73**, 5261–5267 (2007).
108. Quast, C. et al. The SILVA ribosomal RNA gene database project: improved data processing and web-based tools. *Nucleic Acids Res.* **41**, D590–D596 (2013).
109. Caporaso, J. G. et al. QIIME allows analysis of high-throughput community sequencing data. *Nat. Methods* **7**, 335–336 (2010).
110. Avershina, E., Frisli, T. & Rudi, K. De novo semi-alignment of 16S rRNA gene sequences for deep phylogenetic characterization of next generation sequencing data. *Microbes Environ.* **28**, 211–216 (2013).
111. Erb-Downward, J. R. et al. Use of direct gradient analysis to uncover biological hypotheses in 16S survey data and beyond. *Sci. Rep.* **2**, 1–13 (2012).
112. Lee, T. A., Rollwagen-Bollens, G., Bollens, S. M. & Faber-Hammond, J. J. Environmental influence on cyanobacteria abundance and microcystin toxin production in a shallow temperate lake. *Ecotoxicol. Environ. Saf.* **114**, 318–325 (2015).
113. Lozupone, C. & Knight, R. UniFrac: a new phylogenetic method for comparing microbial communities. *Appl. Environ. Microbiol.* **71**, 8228–8235 (2005).
114. Lozupone, C., Lladser, M. E., Knights, D., Stombaugh, J. & Knight, R. UniFrac: an effective distance metric for microbial community comparison. *ISME J.* **5**, 169–172 (2011).
115. Wei, J. X. et al. Graphene-reinforced titanium enhances soft tissue seal. *Front. Bioeng. Biotechnol.* **9**, 665305 (2021).
116. Koo, H. et al. Microbial communities and their predicted metabolic functions in growth laminae of a unique large conical mat from Lake Untersee, East Antarctica. *Front. Microb.* **8**, 1347 (2017).
117. Chang, F., He, S. S. & Dang, C. Y. Assisted selection of biomarkers by linear discriminant analysis effect size (LEfSE) in microbiome data. *J. Vis. Exp.* **183**, e61715 (2022).

ACKNOWLEDGEMENTS

The authors wish to acknowledge the financial support of the work was support of National Key Research and Development Plan of China (No. 2022YFB2603000), Key R&D Program of Shandong Province, China (No. 2022CXPT027), and MIITC High-tech Ship Research Projects (No. MC-202003-Z01-02).

AUTHOR CONTRIBUTIONS

Z.W. drafted the paper and conducted the experimental work under the supervision of X.W. All authors evaluated and visualized the results. X.W. and Y.H. reviewed and edited the paper.

COMPETING INTERESTS

The authors declare no competing interests.

ADDITIONAL INFORMATION

Supplementary information The online version contains supplementary material available at <https://doi.org/10.1038/s41529-023-00365-2>.

Correspondence and requests for materials should be addressed to Xiutong Wang.

Reprints and permission information is available at <http://www.nature.com/reprints>

Publisher's note Springer Nature remains neutral with regard to jurisdictional claims in published maps and institutional affiliations.



Open Access This article is licensed under a Creative Commons Attribution 4.0 International License, which permits use, sharing, adaptation, distribution and reproduction in any medium or format, as long as you give appropriate credit to the original author(s) and the source, provide a link to the Creative Commons license, and indicate if changes were made. The images or other third party material in this article are included in the article's Creative Commons license, unless indicated otherwise in a credit line to the material. If material is not included in the article's Creative Commons license and your intended use is not permitted by statutory regulation or exceeds the permitted use, you will need to obtain permission directly from the copyright holder. To view a copy of this license, visit <http://creativecommons.org/licenses/by/4.0/>.

© The Author(s) 2023